Westfälische Hochschule

University of Applied Sciences
Gelsenkirchen Bocholt Recklinghausen

Masterarbeit

Titel der Arbeit // Title of Thesis

Entwicklung von mikrofluidischen Strukturen in PDMS für modulare, hoch integrierte Lab-on-a-Chip Anwendungen

Development of microfluidic structures in PDMS for modular, highly integrated Lab-on-a-Chip applications

---

Akademischer Abschlussgrad: Grad, Fachrichtung (Abkürzung) // Degree

Master of Science (M.Sc.)

Autorenname, Geburtsort // Name, Place of Birth

Steinchen, Felix // Gelsenkirchen

Studiengang // Course of Study

Mikrosystemtechnik

Fachbereich // Department

Elektrotechnik und angewandte Naturwissenschaften

Erstprüferin/Erstprüfer // First Examiner

Prof. Dr. Michael Schlüter

Zweitprüferin/Zweitprüfer // Second Examiner

Prof. Dr. Hans-Joachim Lilienhof

Abgabedatum // Date of Submission

01.12.2020

Eidesstattliche Versicherung

Steinchen, Felix

Name, Vorname // Name, First Name

Ich versichere hiermit an Eides statt, dass ich die vorliegende Abschlussarbeit mit dem Titel

Entwicklung von mikrofluidischen Strukturen in PDMS für modulare, hoch integrierte Lab-on-a-Chip Anwendungen

selbstständig und ohne unzulässige fremde Hilfe erbracht habe. Ich habe keine anderen als die angegebenen Quellen und Hilfsmittel benutzt sowie wörtliche und sinngemäße Zitate kenntlich gemacht. Die Arbeit hat in gleicher oder ähnlicher Form noch keiner Prüfungsbehörde vorgelegen.

Gelsenkirchen, 01.12.2020

Ort, Datum, Unterschrift // Place, Date, Signature

Abstract

This thesis presents an approach to develop modular microfluidic prototypes including 3-dimensional (3D) microfluidic elements and combining those with electronical sensors in a leakless device. Theoretical structuring technologies are laid out and compared to a method developed in 2015. This method, called ESCARGOT, applies the knowledge of casting microfluidic devices using an elastomer, to create microfluidic structures in a leakless bulk. Furthermore, it presents low cost structure generation using the 3D printing technology. A proof of concept was generated, through the development of basic to more complex elastomer devices that can be used to create Lab-on-a-chip (LOC) applications. In previous research, it could be shown that the advancement of the 3d printing technology can make a decisive contribution to the creation of microfluidic structures [SV15] [Weh16] [Her19]. Inspired by the previous work involving the ESCARGOT method, this thesis takes it a step further to prove that standard microfluidic components like quake valves can also be integrated into the elastomer material. Consequently, integrated logical gates as well as, peristaltic pumps, a droplet generator and a microfluidic mixer were developed. These in turn can be equipped with electronic sensors, as another component presents a monitoring device to measure discrete wavelength with an incorporated optical sensor. A PID controlled temperature controller could also be successfully integrated in a compact elastomer device, establishing short pathways for electrical circuitry and tight temperature control inside the channel. The functionality of these modular Lab-on-a-chip components includes two key elements. The actual lab-on-a-chip system, as well as the bulk material which, as an exoskeleton, encloses the sensors and fluidics. Bulk means that the entire system is made from a coherent mass, which eliminates leakage. The polymer coating of the components defines the external shape and, at the same time, guarantees protection against environmental influences. The whole process was optimized and adapted to the respective applications, to enable 3-dimensional arrangement of the included elements. The processes and components can be modified, multiplied or scaled up as desired using standard design software and generally affordable standard 3D printers. Once the design of these components is completed, mass-produced, single-use products could easily be distributed. The elastomer and the structure-creating 3D filament are safe, inexpensive and can be used by everyone. With this method, microfluidics is no longer reserved for large corporations and can be carried out by anyone.

Table of contents

1 Introduction

In today's world microfluidics are facing the same challenges and problems as electronics faced nearly a hundred years ago. The ongoing demands for smaller and more efficient integrated circuits and micro-electrical components, drove the industry to continuously double the number of transistors in an integrated circuit every two years. This phenomenon known as Moor's law, also relates to a reduction in size, cost, density and the increase in speed of electrical components [Moo65]. Although these factors are all beneficial for the economy, there is still a need for prototyping boards which are created for single purpose applications. These boards are built with a PCB-Layout application. PCB stands for Printed-circuit-board. The same way these boards fill a need in our current society, there is also a demand for prototyping circuits in microfluidics. Microfluidic devices became smaller and more efficient over the years. However, the production cost and time investment to manufacture such devices is too much to bear for small businesses. To be able to afford small integrated microfluidic devices for single purpose applications, there needs to be a similar process as it has been in the electronics environment with prototyping PCB-boards. With this approach, small companies, would we able to develop their own low cost microfluidic prototype devices. An ongoing challenge presents the incorporation of electrical components within the microfluidic device, as well as manufacturing functional 3-dimensional structures. Usually microfluidic devices include a variety of mechanical and detachable components. The goal is to develop devices, which consist just like a PCB prototype, out of a variety of modular elements combined into one unified system. Aiming to develop functional valves and integrating those into more complex microfluidic applications like peristaltic pumps, droplet generators and fluidic mixers, will be one of the main tasks of this thesis, together with the spatial 3-dimensional arrangement of the structures to each other and to the integrated electronic sensor units. Ultimately two examples will be presented in form of an optical analyzing unit as well as a temperature controlling device. In addition to the alignment problems, attempts are made to develop functional prototypes that show the benefits of the presented method.

Before we get to the individual procedures and structuring methods which are suitable for this project, the importance of microfluidic systems in contrast to conventional laboratory technology will be laid out. In microfluidics different physical quantities predominate than in microfluidics. Volume related effects matter less than surface related

effects in a micro-sized environment. An exemplary representation is the capillary action, where a liquid flows through narrow spaces without the assistance or even in opposition to gravitational forces. Gravity is proportional to the mass and therefore to the volume. If the channel is sufficiently small a combination of surface tension and adhesive forces between the liquid and the surface wall, will overcome gravitational forces and enable functionalities such as passive movement, mixing and separation. If the volume of the fluid is significant smaller than the inner walls surface, the capillary motion prevails [Vil20]. For the same reason, laminar flow outweighs turbulent flow. While some effects like laminar flow can be used for applications like flow focusing, other conditions must be created in order to blend two fluids together. These are important factors when designing functional microfluidic devices. Active manipulation of the fluids is possible by means of micro pumps and valves, for which the dwell times are controllable and short. The surface-to-volume ratio increases, which significantly improves heat transfer and the associated temperature control during the process. These properties enable the implementation of a macroscopic laboratory with its functionalities on a chip size. This increases efficiency while reducing the amount of samples required. Less sample volume also reduces the amount of waste being produced. Smaller dimensions also correspond to less material needed to build a system. That would be advantageous both for possible mass production and for prototyping as production costs decrease. Conventional examination methods in laboratories are often time-consuming and expensive. Processing times can range from a few weeks to a few months, as the samples have to be transported, pre-treated and then processed. A high density of functionality on a small chip would contribute to develop portable Lab-on-a-Chip (LOC) devices, which can be taken directly to the site of investigation (Point-of-Care diagnostic[Ven14]). Real-time measurements could be carried out, which also yields the possibility of wireless transmission. Another crucial point is the high degree of parallelization. Instead of one large measuring body, many smaller measuring bodies can each carry out different analyses. Resulting in a large range of detectable substances with the same size of measuring body. Microfluidics is a vast improving field yielding a high potential in new applications for Lab-on-a-Chip systems [Nei19]. While most biological, chemical and bio-chemical experiments are still computed in laboratories, transferring these experiments to a new environment offers the opportunity to conduct new analysis methods and use the advantages of the microscale world [Whi06].

The last 30 years have shown tremendous advances in microfluidics. The technological evolution and important waypoints of the microfluidic development shown in Figure 1. Starting at the invention of the first transistor, which structuring methods and materials are still used for microfluidics to date. Important analyzing methods like the invention of the polymerase chain reaction (PCR) continuously improved temperature control inside microfluidic devices, while newly established materials presented new pathways and structuring methods. Along the way, the invention of 3D printing promised new advances in microfluidic device generation and opened new technologies for faster and low-cost prototyping [Nei19].

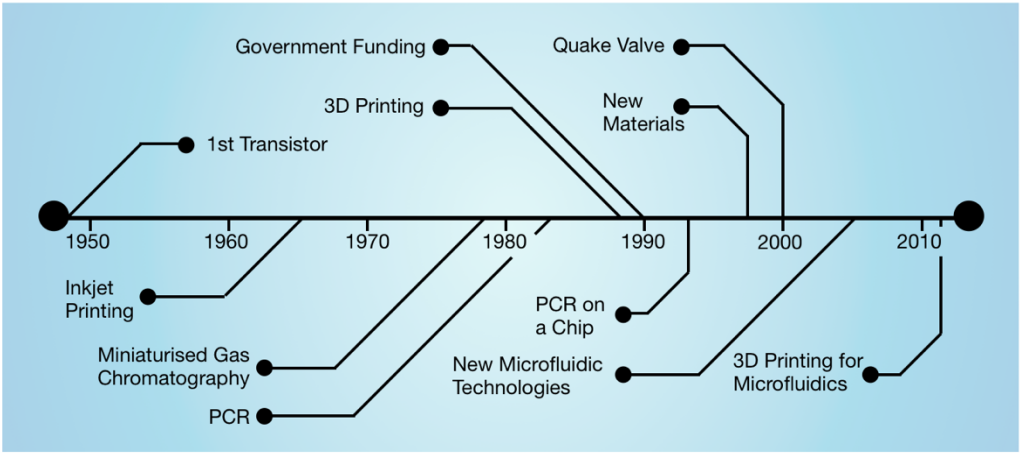

Figure 1: Timeline of the microfluidic development over the past 60 years. Starting with the invention of the first transistor, that marked the beginning of microfluidic development tools as well. Based on the graphic of '30 years of microfluidics' [Nei19].

From the selection of suitable processes to promising materials and the subsequent development of microfluidic devices, some of the terms used in this graphic (Figure 1) contribute and take part in the following chapters and throughout this thesis.

2 Fabrication of microfluidic structures

The development of microfluidics, its materials and its methods is closely linked to other technological areas. The success of microelectronics partly contributed to the success of microfluidics [Hyu09] [Nei19]. In the mid-19th century, integrated circuitry was developed through the invention of photolithography [Xia98]. Which nowadays is still one of the main fabrication methods of microfluidic devices. The materials that are used in microelectronics were also transferred to microfluidics. Since the proceeding of these materials like silicon and glass have already been perfected for microelectronics, the procedures were adapted to manufacture microfluidic structures in the same manner. The following sections will describe and showcase different materials, as well as commonly used structuring methods to determine their suitability for this thesis.

2.1 Materials for microfluidics

There are several reasons for choosing different materials in microfluidics [Pam14]. Each material has different properties which usefulness depends on the application and its requirements. In addition, for most biological and chemical processes it is particularly important that the surrounding material does not interact with the sample and organic solvents. For this reason, structures made of glass and silicone were the first materials used for developing microfluidic structures [Cip12]. During the past decades, new materials were emerging such as elastomers, thermoplastics, ceramics as well as thick-film photoresists. These groups can be categorized into two broad groups: inorganic and polymers. Another important factor is whether the material is transparent. Since many microfluidic processes use optical analysis methods, it is essential that the material in between does not interfere with the measurement method and gives visual feedback. Special system requirements for this thesis are the generation of 3-dimensional structures and the possibility of integrating active components such as valves, as well as incorporating electronical components inside the measuring body.

Inorganic materials like glass, silicon and ceramics are used mostly due to their chemical inertness. However, silicon and ceramics are not usable for optical analyzation methods due to their lack in transparency. Additionally, their rigidness presents a major drawback if active elements like membranes are desired [Emm16]. Nevertheless, there is a workaround for glass and silicon that involves a bonding process with flexible polymer materials. One disadvantage is the fabrication process of these materials, creating only 2-dimensional structures. In order to generate 3-dimensional devices, layer stacking is a

conventional method that resolves this issue. On the other hand, layer stacking as well as adding flexible membrane, involves the need for a plasma oven in order to bond these layers together. Additionally, the process of layer stacking often generates alignment errors and thus low reproducibility. In this regard inorganic materials are not the most suitable choice as an exclusive material and could only be used in a conjunction with a polymer, especially if the incorporation of electronic devices is desired.

Polymer-based materials combine a wide range of mechanical, chemical, optical and electrical properties. Surface properties such as adhesion, coating, surface friction and biocompatibility play an important role in the selection of a suitable polymer in microfluidic applications [Bel00]. They themselves can be divided into elastomers and thermoplastics. Contrary to inorganic material fabrication techniques, processing polymer bodies is relatively simple and involves no hazardous etching reagents. These processing techniques can include a variety of structuring methods like molding, embossing, 3D printing or casting the polymer onto a master structure [McD99]. **Thermoplastics** like poly(methyl methacrylate) (PMMA) and poly(ethylene terephthalate) (PET) are some of the materials commonly used to fabricate microfluidic parts. However, these materials are rarely used for developing active elements like valves due to their lack in elasticity [Emm16]. Even if the presented materials aren't fulfilling the requirements for this thesis, thermoplastics will take on a different role in the later course of the thesis. **Silicone elastomers** are part of the polymer family and often used in biological applications due to their low cost and the variety of processing options. One of these silicone elastomers is Polydimethylsiloxane (PDMS), which is often used in research. Due to its chemical integrity, its transparency and flexibility, PDMS is a diverse material for fabricating microfluidic structures. Especially when it comes to developing prototypes. Additionally, it is possible to bond PDMS irreversibly with another PDMS layer or a glass surface. Due to its elastic characteristics and the ability to enclose other materials PDMS proves to be a particularly suitable material for the described requirements and thus will be examined in more detail in the following chapter.

2.1.1 Polydimethylsiloxane

Polydimethylsiloxane (PDMS) was initially used to enclose electronic components, to protect them from environmental influences [Nei19]. A general advantage is the transparency of PDMS, especially in microfluidic applications the running processes can be observed and controlled. As mentioned above, the chemical inertness of PDMS makes it a suitable lab-on-a-chip candidate in the field of bio-chemical processes as well. Compared to microchannels within very stiff materials such as PMMA, PDMS has a different

modulus of elasticity (resistance to deformation) which is influenced by the curing temperature. This allows to establish deformation-driven structures such as quake valves inside the PDMS structure. Post-separation is one of the problems with PDMS. It is possible to irreversibly connect glass and PDMS or PDMS and PDMS to one another after surface treatment inside an oxygen plasma. The direct deposition of another material like electronic conductor tracks is not possible. An alternative would be to deposit the electrically conductive layer on a glass substrate, to subsequently connect the substrate to the PDMS through the bonding process. However, it is possible to enclose electrical wires and electrical components directly through the process of casting. Casting means pouring PDMS over the electrical elements while it's still in a liquid state. More on the advantages of casting and further development of this technique will be given in the next chapter.

PDMS became, and remains the most common material for device fabrication due to its ease of manufacture and relative low cost. However, the cost of PDMS is often offset by the requirement of a master mold, produced through advanced manufacture methods. Considering PDMS is utilized for fast prototyping production, developing expensive time consuming master structures is a major weakness. There has been a variety of new strategies to structure PDMS and to use it for rapid prototyping, which erase the previous mentioned disadvantages and make it applicable for the presented goals. Especially the option of enclosing electrical modules like sensors and using the elasticity for active components make a suitable material for this thesis.

2.2 Microfluidic fabrication techniques

Depending on the material and application, different fabrication techniques can be chosen to develop microfluidic channels or bodies. If the desired structures involve active working membranes or if on-chip sensor elements must be included, decides the types of materials and thus the structuring technologies being used. An increased amount of functionality and complexity also demands more complex fabrication and combination methods. The oldest technology transferred from the manufacturing process of conventional 2-dimensional integrated circuits (IC) is that of photolithography. While photolithography is suitable for producing small structures with high aspect ratios, there are disadvantages due to the inability to produce complex 3-dimensional structures. It also requires expensive equipment to carry out the photolithographic process [Jin11].

For rapid fabrication of modular, highly integrated, complex microfluidic structures, processes with an expensive master structure or master mold are not qualified. A master structure is usually needed for high throughput and mass production processes. However, due to high costs for creating master structures these methods are not eligible for prototyping. Technologies involving the need for master structures are embossing, where the master mold is usually pressed onto the device-defining material [Bec00] and injection molding, where molten material is injected onto the master structure [Att09]. One of the main materials used in microfluidic fabrication and previously discussed material is PDMS. PDMS is one of the most suitable materials for the design of modular prototypes, due to its adaptability and low costs. The technology of casting is the preferred method when choosing PDMS as a main material. Figure 2 shows how a PDMS device is commonly made [Gui20]. PDMS is poured over a master mold, which presents the fluidic channel structure. After the PDMS has hardened, the master mold can be removed. In addition, in- and outlets are provided at the channel ends by punching or drilling. What remains is the open negative imprint of the structure with its in- and outlets. This can either be enclosed with a layer of cured PDMS or a glass substrate. For this purpose, the surfaces to be connected are treated in an oxygen plasma, increasing the reactivity of the surfaces to subsequently fuse them.

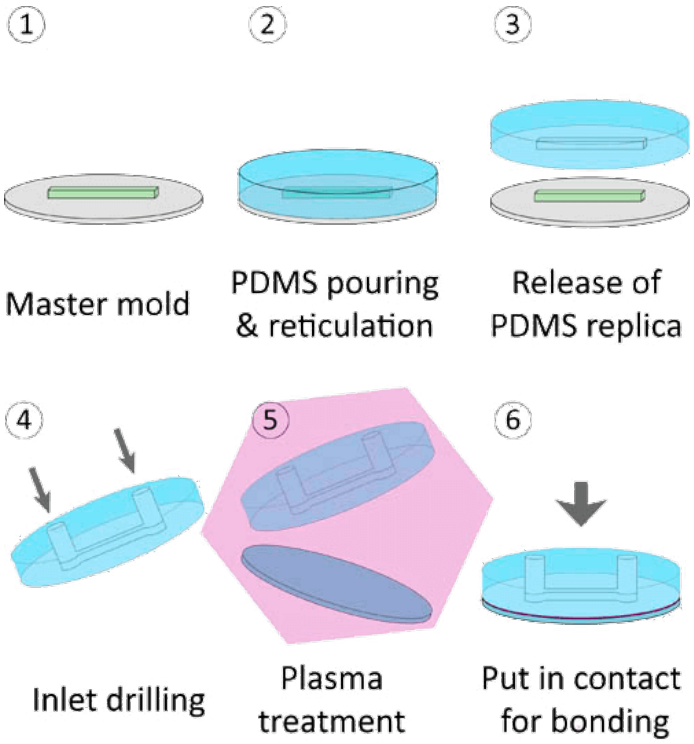

Figure 2: Process of fabricating a basic PDMS device [Gui20].

Nevertheless, this technology is in need of a master structure like embossing and injection molding. This would once more lead to the developing process of a master structure through the already excluded photolithographic process. Next to photolithography, micro milling has the ability to structure master molds as well and is able to fabricate micro channels directly at low costs. However, micro milling has compared to other methods like embossing and injection molding a poor surface quality and is additionally like most methods unable to create complex structures. A possibility to develop complex structures through the process of casting requires multiple PDMS layers that need to be aligned to one another, which results in low reproducibility [Jac05]. A different approach takes the technology of stereolithography, which is able to manufacture complex designs through light curing a liquid photopolymer resin inside a chamber. Apart from the increased complexity, the generated structures are more rigid than those of PDMS. Therefore, it becomes more difficult to establish integrated functional membranes and active elements. None of the methods mentioned above fully meet the requirements. To develop complex 3-dimensional structures, a combination of procedures must be used to achieve the required goals.

However, this is not the only solution to build a device from PDMS. There are two new techniques which have been developed in the past decade. The first technique uses the technology of embedded 3D printing (EMB3D). Here the channels are printed directly into the structure of the PDMS using a fugitive ink [Abi19]. Despite fulfilling the requirement of creating 3-dimensional structures, only a special custom-designed, multi-material 3D printer can be used with the EMB3D method. The second technique has found new possibilities to optimize the casting process to avoid the required master structures as well as layer stacking and at the same time couple 3-dimensional structures with electronic sensors. Such a procedure was developed in 2015 under the name ESCARGOT (embedded scaffold removing open technology) at the Laboratory of BioNanoTechnology [SV15]. It includes the encapsulation process of 3D printed structures, which can be removed by a solvent after the polymer has cured. Since this thesis was written and processed based on this procedure, the properties and procedures will be discussed in more detail in the next chapter.

2.2.1 Embedded scaffold removing open technology

One of the fastest possible ways to develop cheap microfluidic devices is by using the Embedded SCAffold RemovinG Open Technology (ESCARGOT) method. Only three materials are required for a simple fluidic device. A polymer with an initial fluidic state, as the main fluidic bulk material. A malleable, soluble material that forms the channel structure. And a solvent to dissolve the channel structure, without attacking/affecting the polymer. For a method to encapsulate and dissolve microfluidic structures, only materials that can be released after being encapsulated in the polymer body are suitable. In addition, the polymer should have the property of allowing the solvent to penetrate through its structure so that the scaffold can be dissolved from all sides.

The dissolving process is independent of the structure of the material to be dissolved. It can be both simple channel structures or a combination of 3-dimensional layers arranged in various places. If the whole component is lying in the dissolvent bath, everything inside the device will be affected. Consequently, the structure can be as complex as possible as long as fluidic in- and outlets are arranged so that the dissolved material can escape the polymer body. A key point is the smoothness of the surface texture of the enclosed material. This surface is completely transferred into the hardened surface of the PDMS. Evidently the rougher a material is from the outside, the rougher the structure will be within the polymer. Chapter 2.1 described various materials which are used to fabricate microfluidic structures. PDMS shows special properties like its gas permeability which can be advantageous for oxygen and carbon dioxide transport for cellular studies [Eve20]. Furthermore, PDMS is a liquid elastomer before it becomes a firm, elastic body through the consolidation process. For this reason, PDMS was often used for the casting process by pouring PDMS over a master structure. It is precisely this approach that the ESCARGOT method makes use of, by pouring PDMS over complex structures and dissolving them subsequently with a solvent. Which solvent is used, depends on the 3D structure to be generated. The material of the 3D structure partly determines the structuring technology. As with the overall construction of the microfluidic devices from Chapter 2.2, processes such as micro milling, injection molding or embossing can be used to develop the scaffold structure. In order to develop ever more complex structures that are spatially arranged in three dimensions at low cost, the 3D printing process is particularly suitable. Current developments show that increasingly complex and smaller structures can be printed with better resolution [Gri20]. Applying the casting process to these structures establishes a complex structure enclosed in PDMS. Since the solvent should be able to diffuse through the structure of the cured

PDMS, the scaffold structure should be dissolved after an exposure time, to eventually be rinsed out. Choosing a scaffold material depends on the available 3D printing filaments, as well as on a suitable solvent. Solvable 3D printed structures are commonly used to create support structures for reinforcing overhanging bodies. For 3D printers with two extruders PVA[1] is the most frequently used filament, because of its water solubility. Since water cannot penetrate through the PDMS structure, it is unsuitable as a solvent for the ESCARGOT procedure [Wat96]. Common filaments are PLA (Polylactic Acid), ABS (Acrylonitrile butadiene styrene) and PET (Polyethylene terephthalate). However, PLA and PET are resistant to commonly used organic solvents. ABS, on the other hand, can be dissolved with commercially available acetone. Acetone also offers the property of penetrating the filament through the PDMS structure. Therefore, it can be concluded that a combination of ABS with Acetone as a solvent is the best option for the removal scaffold technology. This defines all three components of the ESCARGOT process.

The encapsulation process begins with the preparation of PDMS. After PDMS has been mixed with the cross-linker and degassed, it can be poured over the printed structure. In contrast to the normal casting process, the entire structure is enclosed on all sides. Time dependent curing temperatures can be varied to determine the desired flexibility of PDMS. After the curing process the entire component is placed in an acetone bath for approximately 24 hours. During this time, the acetone diffuses through the structure of the PDMS bulk and attacks the internal ABS structure. 24 hours later, the slightly viscous, dissolved ABS can be rinsed out of the structure with acetone by means of an active pumping process. Due to the elasticity of the PDMS body, the liquid ABS can be pressed out of the entire structure at the same time. Finally, the canal structures are cleaned with fresh acetone and then with isopropanol. In addition to the printed scaffold structures, any other components like electronic sensors or electronic active elements such as electrodes or LEDs, can also be enclosed in PDMS. It is important that the selected solvent does not attack these structures. However, due to the ability of cleaning electrical circuits, which involve acetone as a solvent, most electrical circuits won't be affected. A schematic representation of this process can be observed in Figure 3.

[1] Polyvinyl acetate (PVA) is a water-soluble synthetic polymer.

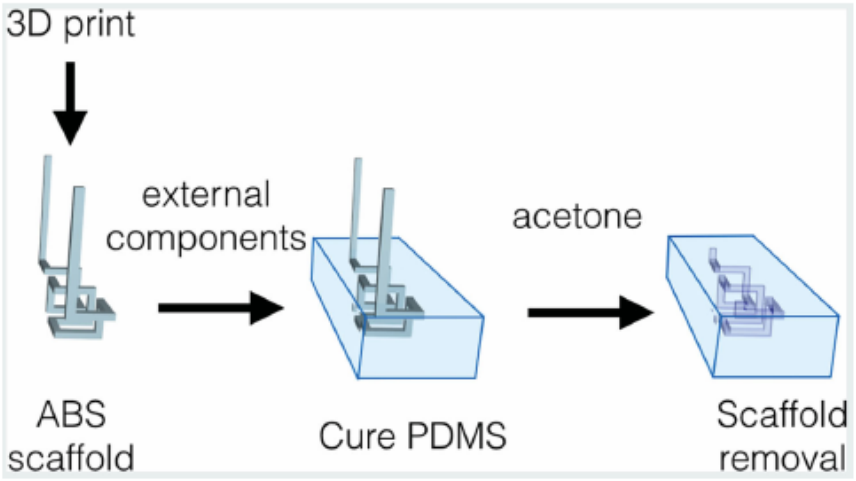

Figure 3: Schematic representation of the ESCARGOT process. Including the design and printing of the ABS scaffold, enclosing it in PDMS and removing/dissolving it in acetone afterwards [SV15]

To develop structures for the ESCARGOT process, commercial printers in the price range from 300 € -5000 € can be utilized. Since the aim of this thesis is to develop cost-effective and quickly creatable modular PDMS devices, the ESCARGOT process will be used. One advantage of the commercial printers is the community and a large range of experience reports and solutions to different approaches, as well as a large base of open source files and data sets for perfect parameterization. This makes the development of microstructures easier and can also be learned very quickly by non-professionals.

2.3 3D printing

Since 3D printing is one of the main aspects of this thesis, a detailed look will be given on the functionality and behavior. In addition, optimization processes are presented in order to produce the smallest possible structures.

3D printers for material extrusion

3D printing was invented in the mid 80's by Charles Hull by using stereolithography [Nei19]. Stereolithography describes the process of stacking two-dimensional laminae to create a three-dimensional body. The object can first be developed on a computer using 3D modelling programs. When the file is exported and converted, the generated body is broken up into individual 2-dimensional layers and can be processed further. The principle is similar to that of a milling cutter, with the difference that it is an additive instead of a subtractive process. For stereolithography the body is being manufactured in an UV-curable resign, that will be hardened layer after layer. Nowadays there are more effective 3D printers and materials on the market that are simplified through the use of open source programs and low acquisition costs. The most widespread printers on the market which are commercially available for a small budget, work on the principle of material extrusion (also referred to as Fused Deposition Modelling (FDM)) seen in Figure 4.

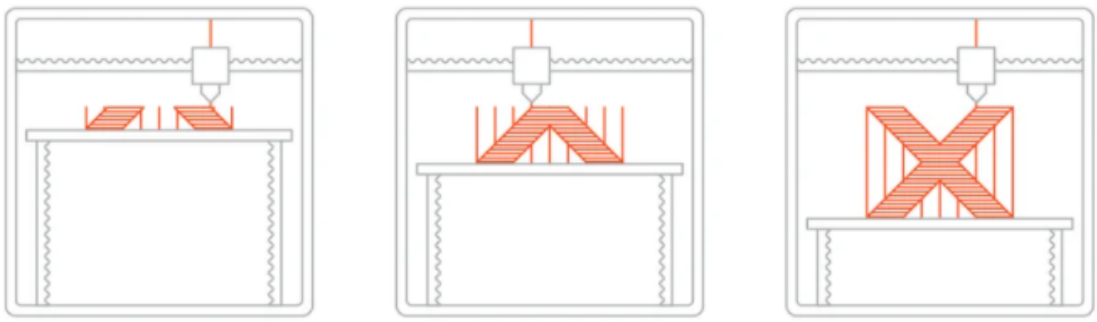

Figure 4: Simple schematic of a FDM 3D printing process. Layers will be added with support structures at overhanging parts [All20]

Here a solid thermoplastic filament is pushed into the print head. Inside the print head, the material is heated until it melts and is pressed through the nozzle onto the build platform. The deposited filament cools down in seconds and becomes a solid body. The print head moves along the programmed path like a milling machine, adding layer after

layer. To achieve increasingly complex structures, support structures can be printed under the overhanging parts. Usable filaments range from materials like PLA, ABS, PET, PETG, nylon to exotic wooden filaments [All20].

Challenges and optimizations involving 3D printing

When it comes to printing structures as small as 500µm or less, different parameterization sets are required than for macro structures. Common complications and errors that occur in the production of 3-dimensional structures are wrapping, oozing/stringing, over-extrusion, overheating, inconsistent extrusion/under-extrusion and layer separation. While the influence of some of the errors decreases as the structures shrink, others increase. Figure 5 shows the most common errors when printing small structures.

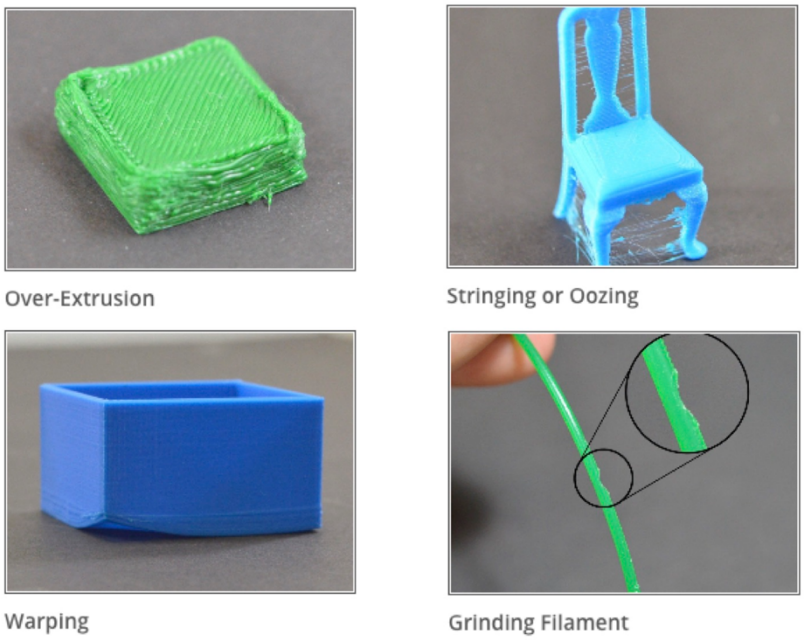

Figure 5: Common errors when printing small structures [Sim20]

Oozing or stringing has a greater impact on small structures. This is caused if the melting temperature for the filament is being set too high and due to the minimal distances between the settling points of the print head. If there are small gaps between the structures, part of the residual material is pulled to the other side of the structure. This creates an unwanted thread of material that is mostly repeated with every shift. For 3D printers, there is a special setting that allows the filament to be withdrawn after the print has stopped. The retraction distance and retraction speed settings are used to pull the filament back into the print head at a certain speed for a certain distance. The faster this process takes place, the faster and cleaner the printing thread leaves the

printed surface. However, a retraction distance, which is too far, can cause the filament to be "grinded". This means that the feed teeth of the filament motor gradually eat their way into the filament and can no longer grip it. Subsequently, not enough material is extruded, which causes under-extrusion. Printing small-scale structures is prone to small changes in the printing temperature. Temperatures that are too high can cause the surface of the printed area to deform shortly after printing before it solidifies. To counteract this effect, print head cooling can be switched on. Cooling the emerging filament solidifies the melted material faster to stay in the desired shape and form. It is particularly important to reduce the speed while printing small structures. This prevents the molten material from being drawn from the print bed too early and prevents small structures from sticking to the print head due to excessive movements [Sim20]. A negligible error is that of layer separation. This occurs when the layer height is chosen too large (mostly for printing big structures in a small amount of time) and the individual layers do not have sufficient adhesion. Wrapping in turn can lift the structure off the print bed, when adhesion is insufficient. This can mostly be compensated in using materials like blue tape or a mixture of acetone solvent on the print bed. A precise understanding of the printer is necessary to print smaller and smaller structures, since fixing one error can lead to another error. It can be assumed that in the future these errors will be revolved and an ever-higher resolution will be achieved, as 3D-printers autolevelling features improve and smaller nozzles are being produced.

3 Developing ESCARGOT devices

The introduction of the ESCARGOT method displayed in the scientific work from the BioNanoTechnology laboratories [SV15] already displayed a variety of example PDMS devices. However, they have mostly dealt with the combination of electronic components with PDMS. Developing functional simple basic microfluidic devices like active valves or peristaltic pumps and comparing those with conventional fabricated devices is still missing. In this section the differences and adaptations required to meet the objectives of this thesis will be laid out. In order to generate the necessary precision to develop these structures, the process must be optimized. A key component will be the fixture that aligns the individual components with one another.

The developing process of a PDMS device with the ESCARGOT method presented in this thesis includes 6 main steps.

1. Designing the fluidic structure and the fixture in a CAD application
2. 3D printing the ABS components
3. Preparing PDMS
4. Encapsulation process
5. Dissolving ABS in Acetone
6. Cleaning the device

Each section presents its own difficulties, which will be explained and analyzed in this chapter. The previous chapter described the optimization of the 3D printing process in detail. It can be assumed that 3D printed structures will achieve an ever-higher resolution in the coming years, as these structures define the internal shape of the fluidic channels and bodies [Fre17]. Today it is already possible to manufacture channels with a diameter of less than 100 µm in commercial environments. However, printing smaller bodies corresponds to less stability, meaning that the components deform under their own weight. Due to this reason the resolution is limited, depending on the entire size and the distance between the holding structures.

Especially in 3-dimensional arrangements, where the distance between fluidic structures defines the properties of active elements, it is crucial to generate reproducible alignments and minimize errors. The most obvious solution is to print a specialized fixture for every new device, which holds all components in place. A major advantage of the ESCARGOT process is that it creates leak-free devices through the possibility of casting in silicon hoses. Therefore, a possible solution had to be found to firmly integrate the fluidic

connections into the PDMS body. One possibility is to design conically formed ends at the in- and outlets of the printed fluidic structures. The silicone hoses could thus be connected to the structures and the fixture through pressing the hoses on the conically formed connections. However, the hoses are quite flexible and cannot be used to align the structures to one another. In order to connect the fixture to the internal structure, a solid body is needed that fits through the silicone hoses and has standardized dimensions. Another possible solution is using syringe heads. These are commonly used as connection adapters for silicone hoses in other projects and are standardized and defined in the ISO 7864 norm [ISO16]. Connecting them to the Fixture and the internal channel structures presents a design issue that can be resolved before the 3D printing process. This will be achieved through designing a press fit, which will be placed on the fixture side to accommodate and hold the syringe head. The connection between the syringe head and the fixture is shown in Figure 6.

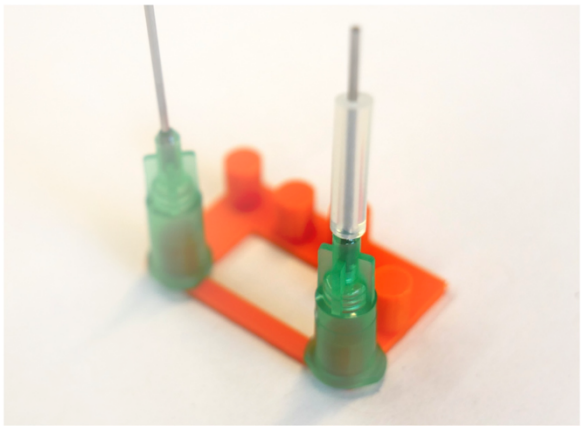

Figure 6: The orange ABS fixture is connected with the syringe needle. This is an upside-down view. For the enclosure process with PDMS the fixture will be turned around with the needle tips facing downwards.

Another press fit is generated on the opposite site of the syringe which can be seen in Figure 7. After the curing process these ensure that the fixture can be easily detached from syringes. Most of the fixtures surface represents the body size. To be able to pour PDMS onto the fabricated structure most fixtures were designed with a gab in the middle, without loss of stability. This also reduces the printing time as well as the amount of filament needed. After the curing process the needle can easily be detached from the device, while the hose is still in place and establishes a solid connection to the fluidic channel. Another characteristic of the channel design are the supporting structures surrounding the ABS channel on the lower side of Figure 7. These structures hold the printed syringe-holder towers in place because the higher these structures are the

more leverage they have. Since each tower is printed simultaneously the cooling material gets dragged each time the print head switches its position. These supporting structures have to be removed manually before proceeding further.

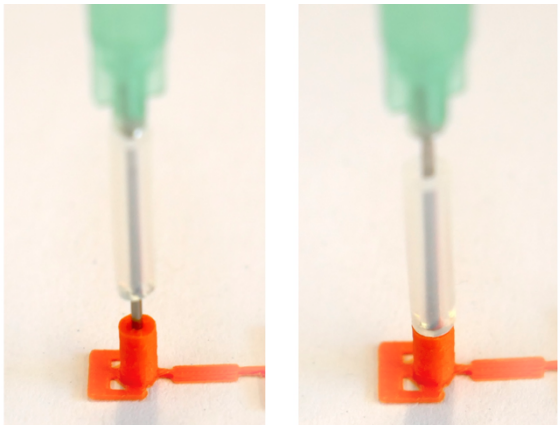

Figure 7: The press fit of the needle ends inside the orange ABS scaffold representing the fluidic channels.

The next step will be the preparation of PDMS, before pouring it over the ABS structure. The appropriate parameters for preparing PDMS, can be derived from the silicone manufacturers technical data sheet (SYLGARD 184 Silicone Elastomer [DOW20]) and from the experience of the Laboratory of BioNanoTechnology [SV15]. Consisting of two components, a mixing ratio of 10:1 (PDMS to cross-linker ratio) must be adhered to. Changes in this mixing ratio have an impact on the behavior of the cured PDMS. In addition to the mixing ratio, various cure times are given, which indicate the curing temperatures for the respective curing time. After mixing PDMS with the cross-linker for about 5 minutes (depending on the amount of PDMS; usually for less than 50 grams), the mixture needs to be degassed in a vacuum chamber for about 30 minutes.

For the encapsulation process, the ABS structure must be fixed, freely hanging in a container. Glass carriers, which are connected to one another with hot-melt adhesive, are particularly suitable as vessels. This allows the component size to be determined, and at the same time makes it easier to remove the component later on, as the hot glue can be dissolved in acetone. If the structures are placed inside the glass carrier vessel, the degassed PDMS can be poured over the structure. The following step of curing (whether at room temperature or in the oven) affects the mechanical properties of the PDMS structure. The higher the curing temperature, the greater the modulus of elasticity (Young's modulus). This means that the resistance that the material offers against elastic deformation increases and the material is therefore less flexible. The curing times

to the corresponding temperatures and young modulus can be viewed in the attachment section of this thesis.

For functional membranes and other active elements, it is recommended to cure PDMS for 48 hours at room temperature, to keep it as elastic as possible. Therefore, membranes are more robust and less energy is needed to actuate them. After curation, the PDMS body can be released from the vessel structure. The final mechanical properties are achieved after approximately 7 days [DOW20]. For this reason, every measurement and test has to be conducted after this waiting period. Depending on the complexity of the structures, the enclosed air bubbles need more time to reach the surface.

Next, the hardened PDMS -with the still enclosed ABS structures- is placed in acetone. Depending on the location of the structures and the arrangement of the in- and outlets, the release process takes about 24 hours - 48 hours. After this period, the ABS is partially released and the flushing process can begin. For this purpose, the individual channels are repeatedly pumped through with a syringe filled with acetone. This process continues until the last remaining ABS has disappeared from the PDMS structure. Afterwards, the channels can be cleaned with isopropanol and dried with compressed air.

4 Developing active microfluidic devices

Lab-on-a-chip devices can be used for almost every biological and chemical application. Before developing any device, considerations must be made which microfluidic components a Lab-on-a-chip system would need to successfully execute its task. In addition to various channel shapes, channel crossings and connection channels, the device needs to fulfil a purpose. This purpose could be the analyzation of a reagent or mixing of fluids. In order to integrate the entire device as far as possible, all the necessary control and analysis systems must be integrated into one chip. Ensuring not only more portability, it would also increase the security against leaks as well as create a low-cost prototyping device. The ESCARGOT method already proved that it can be used to integrate sensors and other electrical components [DOW20]. It has yet to be proven that the same shapes and functional microfluidic structures can be generated with this method, as it is possible with conventional processes. Valves are one of the fundamental microfluidic manipulation methods to control and operate fluids. Next to passive valves that control the fluid through micro-sized effects like the capillary motion, active controlled valves are of great interests when microfluidic systems require complex fluid maneuvers [Adi20]. Integrating these valves and combining them into more complex functional application will be the goal of this chapter. Before the design will be laid out the type of active valve has to be decided.

4.1 Active microfluidic valves

Active microfluidic valves can be divided into mechanical, non-mechanical and external valves. Since most valve types can be used to perform similar tasks, it is more a matter of preference which type to use. These preferences can be depended on which actuation energy source is available or meets the desired properties. Traditionally, mechanical active micro valves are accomplished using the MEMS-based bulk or surface micromachining technologies, where mechanically movable membranes are coupled to magnetic, electric, piezo-electric or thermal actuation methods [Imr07]. Unconventionally, non-mechanical active micro valves can be operated by the use of smart or intelligent materials. These non-mechanical active micro valves may hold movable membranes which are, however, actuated due to their functionalized smart materials such as phase change or rheological materials [Imr07]. Since the aim is to develop a valve mechanism using the surrounding bulk of PDMS and integrating them further for more complex actuation methods, mechanical and non-mechanical methods are avoided. A suitable actuation method is represented by external active micro valves. These are actuated by the aid of

external systems such as built-in modular or pneumatic means. Using external systems is one of the most practical approaches in designing micro valves. This actuation is advantageous with no leakage flows at high input pressures, due to the separation of the control and fluid channel. However, miniaturization may be difficult due to the requirement of additional external system. Additionally, pressurized valves show minimal hysteresis characteristics as has been shown in [Mar00] and are therefore particularly suitable.

4.2 Quake valves

One of the most common micro valve types in microfluidic applications is the quake valve. A quake valve uses the pressure-driven deformation of a soft membrane lying on top of a fluidic channel and blocking or opening it when actuated.

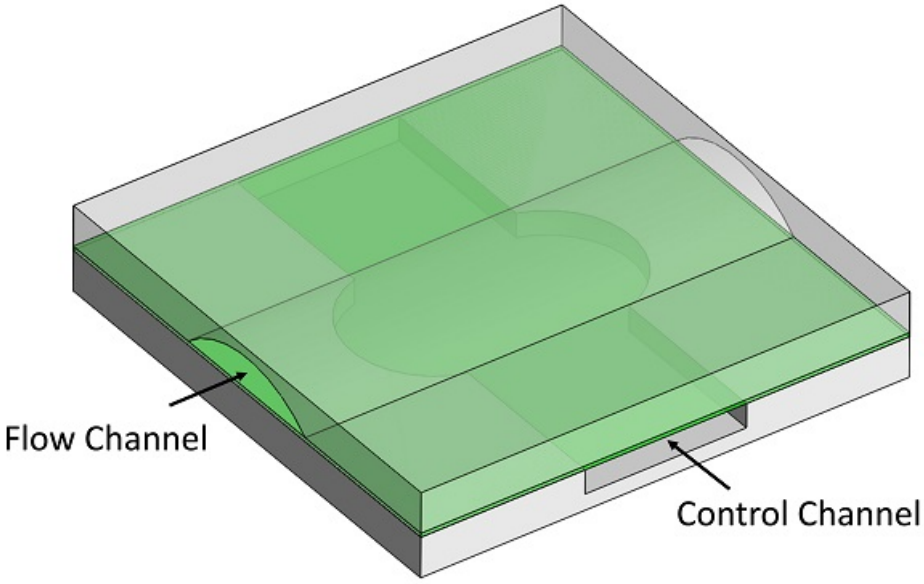

Figure 8: Basic quake valve. Usually the control channel is controled by air pressure. [Ver20]

Differences are mostly visible in the design of these valves. While PDMS is the material of choice to manufacture the flexible membranes [Bro20], there is a divergence in applying these membranes to the surrounding structure. While some groups of scientists use a combination of structured glass and PDMS solely as a membrane material to form microfluidic valves, others are fabricated by using a standard multilayer soft-lithographic technique for structuring PDMS directly [Xia98]. A simple valve would consist of a multilayer completely out of PDMS. The first and third layers are two intersecting

channels, which are separated from each other by a middle layer (the switching membrane; commonly $< 100\mu m$ thick) [Mar00]. Pressurization of the control layer/channel deflects the membrane into the flow channel and thus closes the valve (Normally Open Valves). In another scientific work, it was shown that pneumatically controlled microfluidic microprocessors could be generated by integrating such control elements [Min09]. The integration reduces the complexity of additional connections and devices outside the system. Figure 8 shows a simple multilayer quake valve. The first and last membrane could either be channels etched in glass or molded in PDMS as mentioned before.

Another way to control these valves is the usage of a vacuum (pressure below the local atmospheric pressure). Instead of a membrane that is bulging out, the membrane is sucked in. In consequence, the flow channel is opening (Normally Closed Valves). Parameters that describe the pressure which is needed to deform the membrane are the stiffness, the diameter or length of the membrane as well as the thickness.

4.2.1 Designing a quake valve

While the main difference is the default state in actuation, it has certain benefits to use a normally open valve (NOV). The structure of NOVs is simpler and easier to fabricate. If we keep in mind that the design is dependent on the scaffold removing technology (ESCARGOT), it is difficult to manufacture a normally closed valve (NCV) without using multiple PDMS layers and the associated bond process.
Another point when designing a suitable quake valve is the type of actuation. Since pressure-driven deformation is sought, the fluid channel must be entirely closed when the pressure is active. A purely rectangular channel would still leave gaps at the edges through which the liquid can move. With a semi-circular design as shown in Figure 9 (b), the membrane can be completely inserted into the fluid channel and close it. The second possibility would be to form a thin channel. With enough pressure, the entire canal would pull together, when the membrane presses on the semicircle from above (shown in Figure 9 (a)). These designs are known as push-up and push-down valves [Vin04]. The design always depends on the application. A rectangular channel could be utilized as a sieve filter as has been shown by [Chu05].

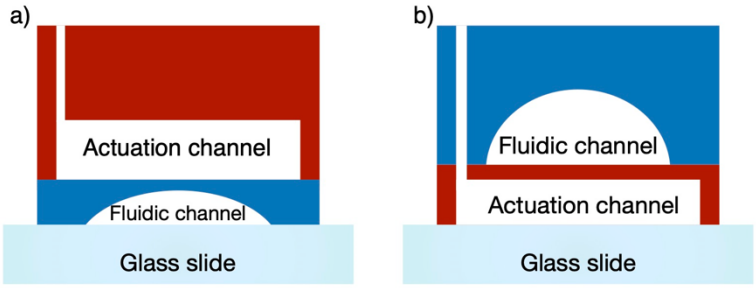

Figure 9: Based on the design of [Vin04]. (a) Design of a push-down valve. The actuation channel/chamber deforms downwards closing the fluidic channel when pressure is applied. A large aspect ratio is required for the fluidic channel. (b) Design of a push-up valve. Applying pressure in the actuation channel deflects the membrane upwards inside the fluidic channel and thus closing it.

4.2.2 Simulation

In order to determine the optimal pressure that is necessary to generate a pressure driven membrane, a valve is designed in Autodesk Fusion 360. The simulation-modules designed in Fusion 360 can afterwards be transferred directly to the 3D printer. The simulated structure is presented in Figure 10.

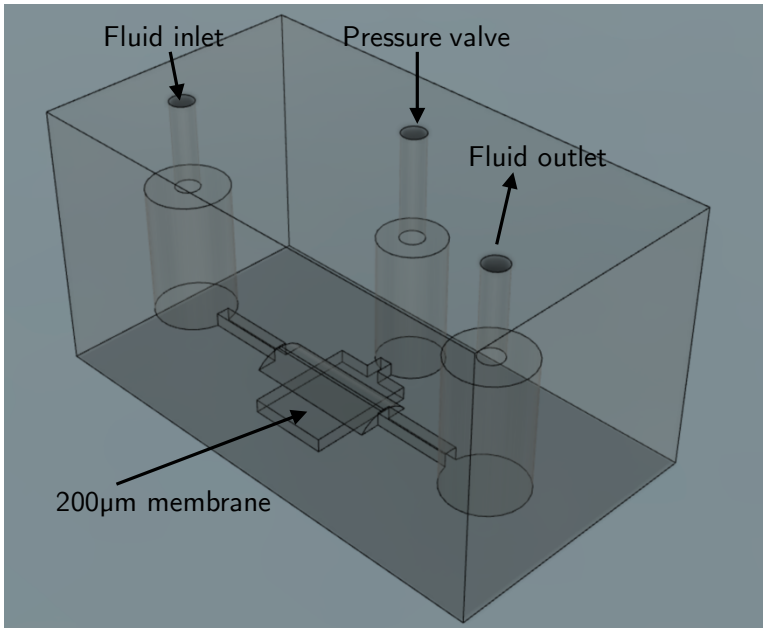

Figure 10: The design of the test quake valve. To test the functionality of the design a simulation will be computed to calculate the optimal valve pressure.

The design of the channel was constructed to correlate with usual quake valve sizes. The size ratio was adjusted, due to deviations caused by the adjustments, as well as due to the minimal printable structure sizes. A transient structural simulation was conducted applying pressures up to 3 bar. The simulation has shown that a valve with 3D printable dimensions could be actuated with a pressure of ≈2 bar to deflect the membrane and close the channel properly. In Figure 11 the pressure deformation can be seen, as well as the displacement value of 479 µm in the center of the membrane. While Figure 11 (a) shows an amplified deflection, (b) shows the actual deflection. On the right side the displacement magnitude bar is given, which displays the distance of deflection from the origin. In Figure 12 the pressurized actuation channel is shown, while the fluidic channels coloring is hidden. The largest deformation takes place directly below the semi-circular channel, due to the least resistance. The simulation was conducted in ANSYS AIM 19.2v. Parameters from the Sylgard 184 datasheet were used to describe the mechanical behavior of cured PDMS [DOW20].

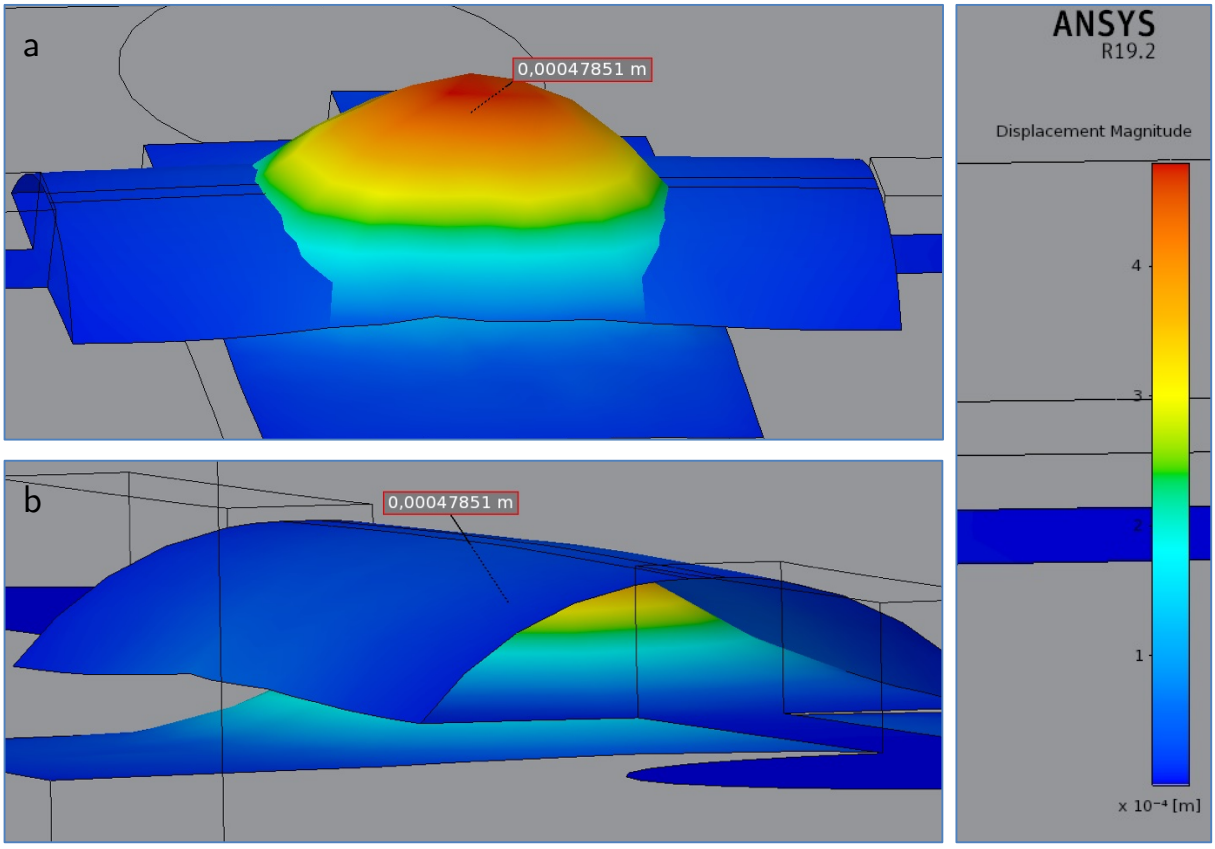

Figure 11: Simulation of the constructed quake valve. (a) shows the deformation of the membrane under the fluid duct. The deflection is shown with a gain factor for illustration. (b) shows the actual deflection of the pressurized membrane inside the fluidic channel. On the left side, the displacement magnitude is shown.

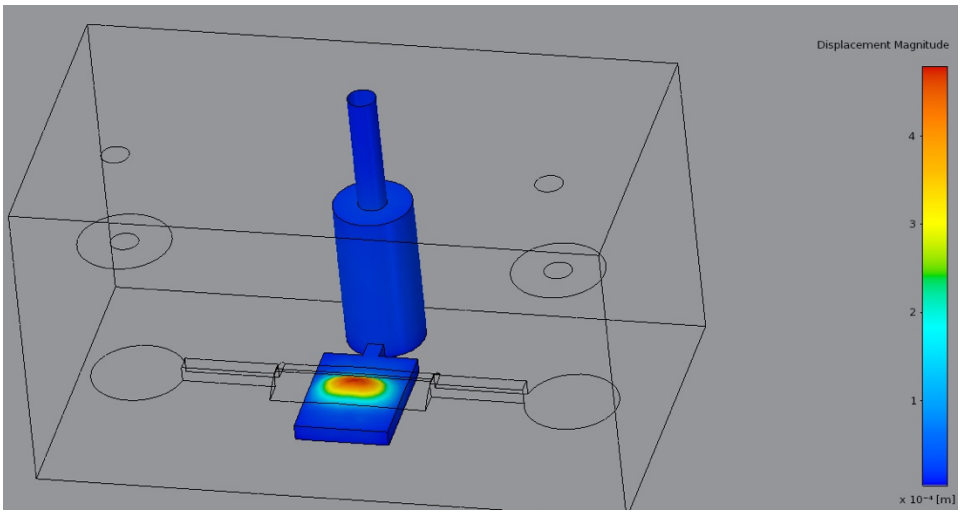

Figure 12: Shows the deformation of the entire pressurized channel. The Membrane is directly above the read area, which displays the maximal deformation point of the valve.

The simulated behavior has been confirmed in practice through the design showed in Figure 10. The pressure was applied through the inlet marked with "pressure valve". Consequently, the membrane deformed through the pressure of 2 bar and dropped into the semicircle of the fluid channel. This closes the channel and liquid flow is being blocked from in- to outlet.

4.3 Additional materials and controlling devices

The off-chip valves are controlled by an Arduino mega 2560. Syringe heads serve as connecting pieces to the off-chip channels with the on-chip channels. These have a thicker needle diameter to generate a leak-free connection.

4.4 Pneumatic logic gates

Now that we are able to manufacture fully functional quake valves in a bulk of PDMS, further integration can be performed in the form of basic logical gates. Logic gates are well known in the world of electronic devices, as they are one of the main components [Jae10]. Computers work in a binary system, that means information as well was operations are usually a combination of ones (Bit 1) and zeros (Bit 0). This way they can communicate, solve equations or create oscillators. A gate has one or more inputs. Each input can represent a high level (1) or a low level (0), which themselves represent a high or low voltage level. Transferring this to quake valves, a high pressure sets an input to 1 and a valve with atmospheric pressure to 0. Depending on the functionality of the gate, it can output a high or low level signal itself.

An integrated logic AND gate and OR gate consists of a total of 3 quake valves, an inlet of atmospheric pressure (atm) and the actuation pressure (P). Two of these valves represent the inputs and one of these valves represents the output. Depending on the status of the valves, 1 (high = switched) or 0 (low = unswitched), the output reacts accordingly. Observing Figure 13 and Figure 14 reveals the schematic design of the AND and the OR gate with their respective actuation tables (logic table).

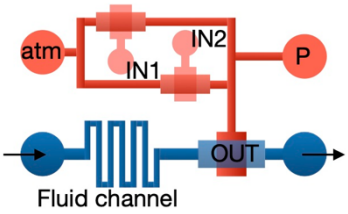

IN1	IN2	OUT
0	0	0
0	1	0
1	0	0
1	1	1

Figure 13: Schematic design of the logic AND gate (left). Actuation table (right).

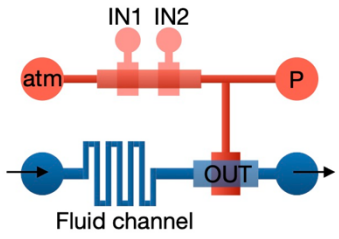

IN1	IN2	OUT
0	0	0
0	1	1
1	0	1
1	1	1

Figure 14: Schematic design of the logic OR gate (left). Actuation table (left).

For an AND gate the output is only actuated if both inputs are switched. If both channels are actuated they close the pneumatic channel. Therefore, the constant pressure coming from the P-inlet can't escape through the atm-inlet. This means that the pressure is applied to the output membrane and therefore closes the fluid channel. This is showcased in Figure 15 (c). The red circle shows the OUT-value representing the pressurized output. If only one of these inputs is being actuated, the pressure still escapes through the open pressure-channel connected to the atm-inlet and the OUT-value is 0 (Figure 15 (a) and (b)).

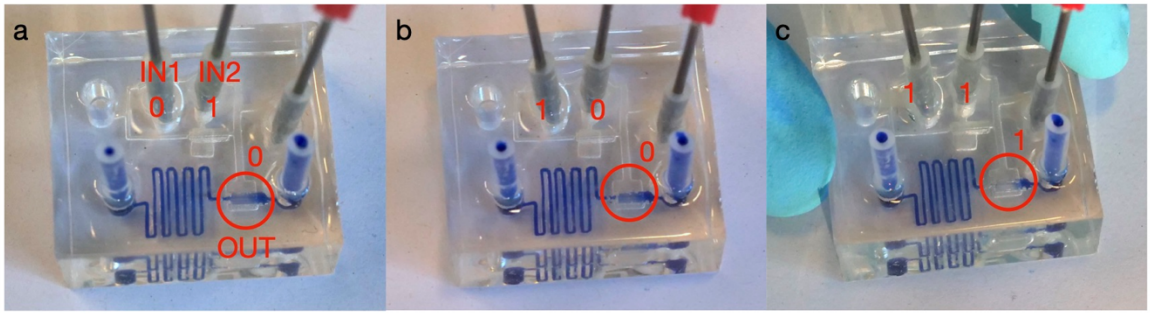

Figure 15: (a) Inlet IN2 is pressurized. OUT is open (b) Inlet IN1 is pressurized. OUT is open (c) Both inlets IN1 and IN2 are pressurized, thus the output OUT is pressurized as well and closes the fluidic channel

The OR gate has a different arrangement of the input valves. Both valves are connected in series. This means when one or the other valve or both are switched, the output valve is supplied with pressure from the act-inlet and the fluidic channel closes (Figure 16).

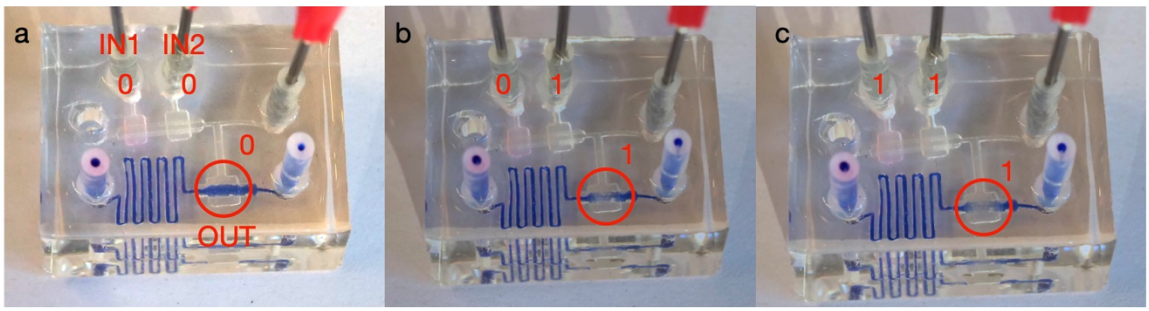

Figure 16: (a) Inlet IN1 and IN2 are unpressurized. OUT is open (b) Inlet IN2 is pressurized. OUT is closed, since pressure can't escape through the atm-inlet (c) Both inlets IN1 and IN2 are pressurized, which has the same effect as (b).

4.5 Peristaltic pump

The designed quake valves can be used for several other applications, such as peristaltic pumps. A peristaltic pumping mechanism is created, if at least three of these valves are controlled serially. In Figure 17 (a) you can see a schematic example of a commonly used peristaltic pump for microfluidic applications.

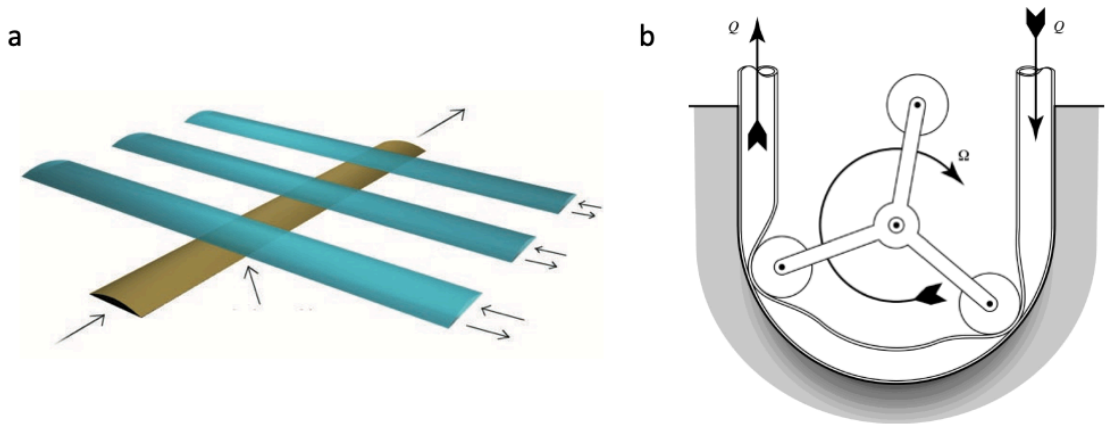

Figure 17: (a) design of peristaltic pumps in most microfluidic applications through the implementation of quake valves [Mar00]. (b) design of a common peristaltic pump for off-chip fluidic applications [Jor08]

The peristaltic method is as simple as it is effective. The Fluid is supplanted by a sinus like wave motion of the actuator. Off-chip peristaltic pumps usually use a rotary motion to convey the liquid through a hose. Two or more cams move on a circular path. At the end of each cam the hose is squeezed, which displaces the liquid in the direction of rotation shown in Figure 17 (b) [Jor08] [Lip93]. While this pump executes a linear rotary movement to convey the liquid, the linearity of the diaphragm pump is dependent on the frequency. The faster the membranes are activated and deactivated, the more linear the flow rate. Since the inertia of the liquid is not sufficient to flow back when one of the membranes opens. That means that the liquid is pushed forwards continuously.

4.5.1 Operation principle and measurements

In various scientific works, different switching sequences are used, which are stimulated at different frequencies [Mar00] [Jac05]. To validate the functionality of the developed peristaltic pump, measurements of the flow rate in relation to the switching frequency

are recorded. These measurements will then be compared with other researched measurements to determine whether similar or even higher pump rates can be generated and how reproducible these flow rates are. For the measurements, the peristaltic is actuated with a minimal step size in frequencies of 0 Hz to 200 Hz. 2 bar is the minimum pressure to fully actuate a quake valve, derived from the simulation in chapter 4.2. To investigate different pumping rates at higher pressures another measurement will be conducted using 2.5 bar. Pressures above 2.5 bar are prone to damaging the membrane.

Figure 18 shows the measurement setup. In front of and behind the peristaltic there are buffer reservoirs which simplify filling. the fluidic sample is countered with a syringe to the starting point of the measuring section. With each measurement, the time is stopped until the measuring section is completely filled with the fluid.

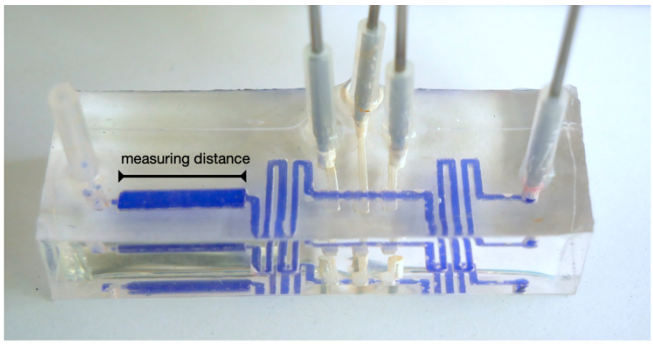

Figure 18: Peristaltic measurement body. Showing the measurement distance (measurement volume) on the left.

The switching times can be seen in Figure 19. The specified frequency is the minimum time step within the programmed code for controlling the valves. This means that the time between valve 1 and valve 2 correspond to the specified frequency. The recurring sequence is repeated every frequnecy times 5, since the frequency represents only one step.

Figure 20 shows that the flow rates initially rise relatively linearly up to a frequency of 40 Hz. After that, the flow rate drops slightly on both conducted measurements. Both at 2 bar and 2.5 bar, resonance frequencies in the range of 60 Hz are found. It can be assumed that the external magnetic valves encounter a resonance frequency. A resonance of the PDMS membranes is rather unlikely at frequencies of this magnitude. This is also supported by the scientific studies compared, in which no resonances from the quake valves were observed [Yua18] [Mar00]. Then the flow rate increases again up to a maximum of approx. 75 Hz. From then on the curve flattens out further and further.

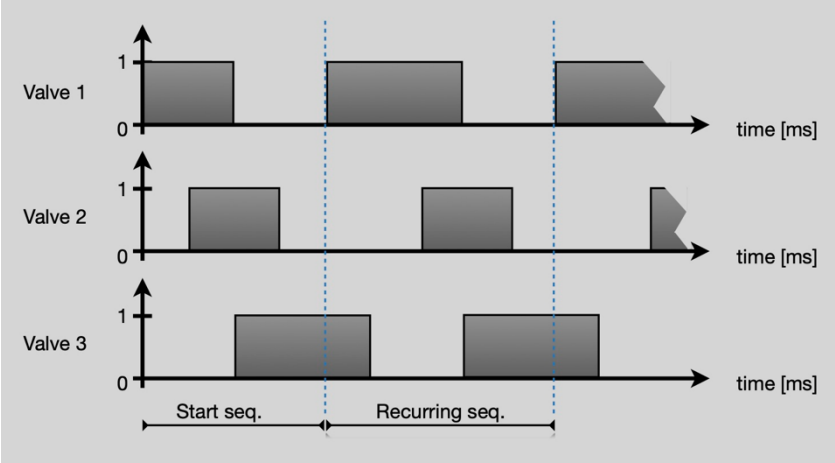

Figure 19: Switching sequence of every valve. The starting sequence is run once at the beginning. The following sequence recurs every period as long as the pumping mechanism is active.

At high frequencies, a pressurization value of 2 bar causes the flow rate to decrease more rapidly than with a pressurization of 2.5 bar. It can be assumed that the reason lies in the reduction of the expansion of the quake valves and thus the reduction in the displaced fluid. This finite-time response of the actuation circuit (the external magnetic valves) is at its limit at ever higher frequencies. That means the membranes are under constant pressure and the flow rate goes to zero.

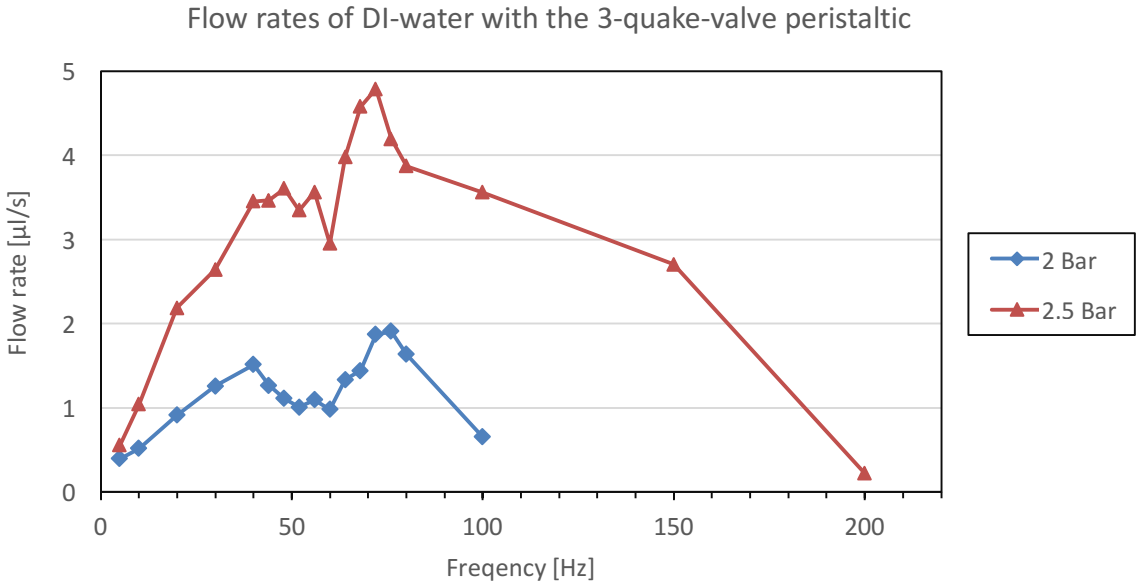

Figure 20: Graph of the flow rates in [µl/s] over the frequency in [Hz]

The pressure valves that supply the quake valves with pressure reach their limit frequency from a slack time of 100 Hz. Apart from the measurement of resonance frequencies, the same results have also been reported in other scientific work [Mar00] [Jac05]. It can be concluded that the highest possible pumping rate of 4.79 µl/s could be attained at a frequency of 72 Hz for 2.5 bar and a pumping rate of 1.87 µl/s at a frequency of 76 Hz for 2 bar.

4.6 Droplet generator

As can be seen, each chapter combines elements from previous chapters, which shows how easily individual elements can be combined in this process to create subsequent elements. The droplet generator combines the peristaltic Pump with a crossroad fluidic section and a reservoir/chamber to gather the droplets. There is a wide variety in applications for droplet generators, such as an ultrahigh-throughput microfluidic screening platform as shown in Figure 21 [Jer10].

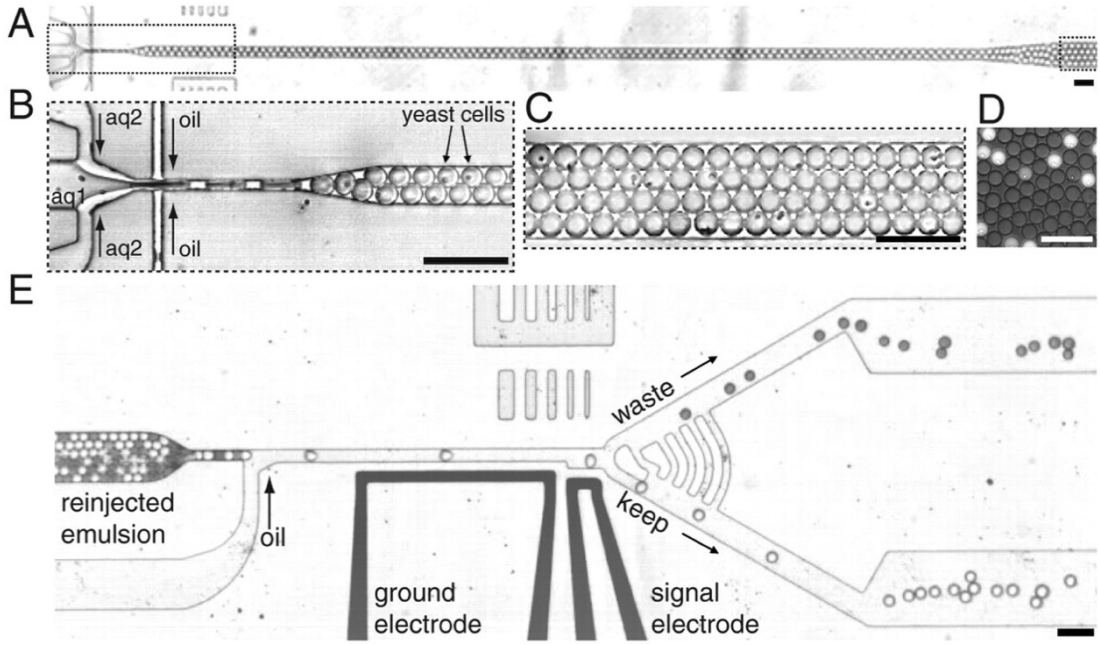

Figure 21: Ultrahigh-throughput microfluidic screening platform. Example application of a droplet generator. (A) Image of the entire channel structure. (B) Magnify the intersections to create the yeast cells encapsulated by two liquids. (C) shows an enlargement of the reservoir. this is where the yeast cells are located. (D) after an incubation period, the filled cells show fluorescence (E) Here the individual drops are separated by oil and all empty cells are sorted out by the electrodes. To do this, a lens is pointed at the cells. The medium filled with the fluorescent substance shine brighter than the empty cells and are sorted out by dielectrophoresis [Jer10].

4.6.1 Operation principle and measurements

Both media, i.e. the surrounding medium (oil) with a higher viscosity, as well as the sample liquid (dissolved colorant), are pumped to the intersection at a continuous pumping rate (Figure 22).

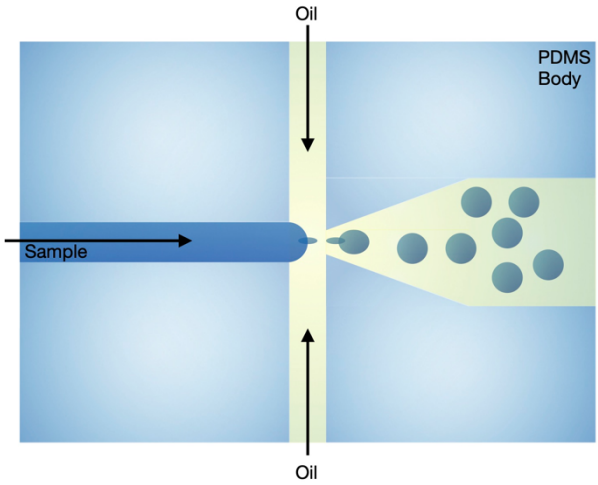

Figure 22: Schematic example of the droplet forming process at the crossroad

The oil cuts off the sample liquid from both sides so that the same sample volumes are generated for each repeated process. The generated drops are then kept in a reservoir. Varying the droplet size and the number of droplets in the reservoir can be changed, when using different flow rates for both fluids. A higher flow rate of the sample would expand the size of the droplets, whereas a higher oil flow rate would have the opposite result. Creating sequential higher and lower flow rates, can increase or decrease the number of droplets. If the reservoir would be as narrow as a flow channel, the droplets could be positioned behind each other. The Distance between these droplets can then be varied through flow rate as well as by stopping the pumping motion of the sample fluid occasionally. An image of the droplet generator can be seen in Figure 23. On the right side the peristaltic pump pushes the liquid to the cross-section, where it meets the barely visible oil channels and gathers the droplets in a chamber.

In the previous section, it was shown which possibilities this process has and how the generated droplets can be used further. In this work, only the generation of these droplets is being demonstrated with an integrated peristaltic pump. The supply of the oil could also be fully integrated by another peristaltic pump. The cell sorting methods

shown in the scientific work in Figure 21 [Jer10], can also be included in the future by pouring in the sorting electrodes in the PDMS structure as well.

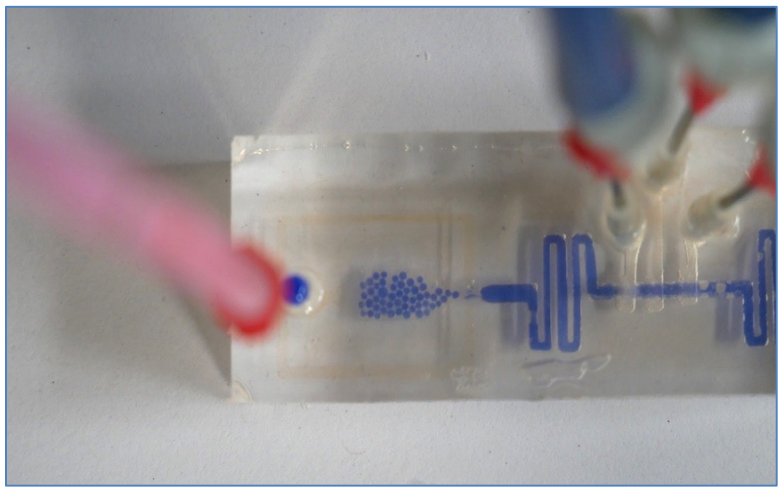

Figure 23: Droplet generator: A fluid is pumped from right to left by a peristaltic quake valve. From the other side of the device Oil is infused by a syringe pump and split up in two channels. At the crossroad, the two oil channels form the fluid in a droplet shaped volume and push it into a collecting chamber.

For the proof of concept, the peristaltic was controlled with a frequency of 50 Hz with a quake valve pressure of 2 bar. The syringe pump that directs the oil to the intersection is operated with a flow rate of 20 µl/s.

4.7 Microfluidic mixer

A mixing device is usually referring to a bowl or a blender filled with liquids that almost mix instantaneously when they are poured into a bowl. In microfluidics two fluids which are infused in the same channel won't mix instantaneously like expected. Due to very laminar flow, there is only little diffusion mixing at the interlayer connection. However, there are different ways to merge two or more fluids with one another in a microfluidic device. A distinction can be made between passive and active mixers. Passive microfluidic mixers involve static structures that enhance the mixing process like a Y shaped inlet or structuring a channel to create different flow speeds and cross-sections. While these methods take more time due to diffusion than active methods, they can be enhanced through varying the flow rate. In general, these methods would be suitable if active elements are to be dispensed with entirely. That could be the case if the complexity of the component is to be reduced or to eliminate the energy that is necessary to stimulate the active mixture. Active mixing processes include methods like the use of ultrasonic waves, thermal actuation, magnetic fields and mixing through pressure actuation [Eve20]. While these methods have their certain benefits and complications, this thesis will solely focus on pressure driven actuation. To show that the derived quake valves as well as the peristaltic motion can be cooperated to fabricate an increased complex and integrated device as shown in the design of Figure 24.

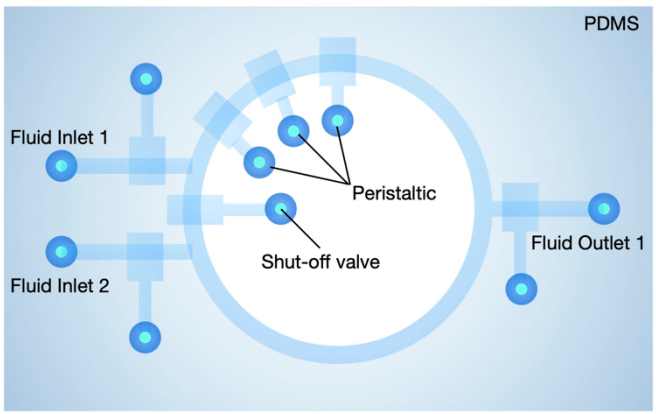

Figure 24: Design of a microfluidic mixer. There are two fluid inlets and one fluid outlet for the mixed sample. The shut-off valve prevents the two fluids from entering the other channel. This creates a mixing ratio of 1:1.

4.7.1 Operation principle and measurements

The PDMS designed microfluidic mixer is a combination of quake valves to create the peristaltic motion as well as basic shut-off valves to close the different pathways (Figure 24). Two defined volumes of fluids are combined in a 1:1 mixing ratio. The left side of Figure 25 shows two inlets for each fluid. Each channel has its own valve to close the connection to the fluid supply. To establish a barrier at the connection point between the two liquid channels, another valve was placed in between.

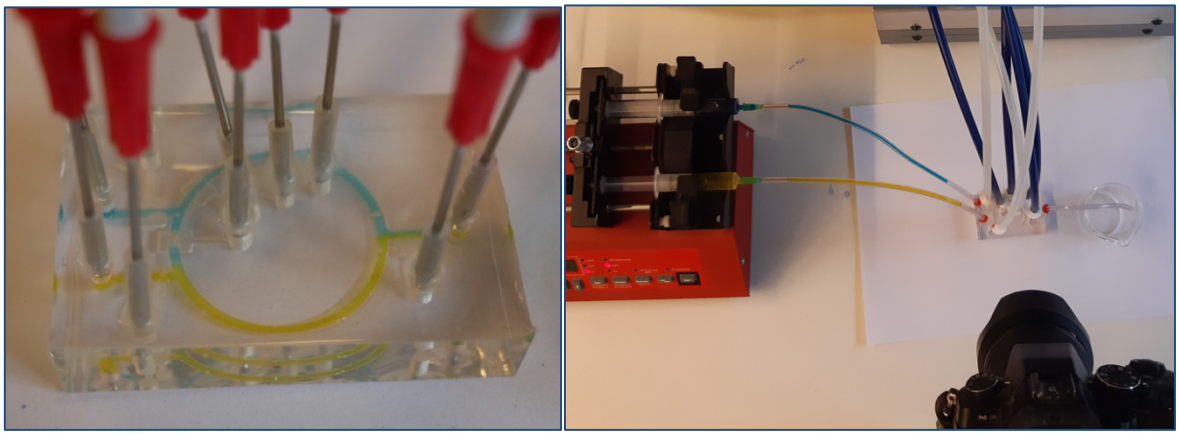

Figure 25: Microfluidic mixing device. Two fluids (blue and yellow) can be inserted on the left side. After closing the in- and outlets, the peristaltic movement is mixing both fluids.

The three stimulating peristaltic valves are located within the mixer loop. To start the mixing process (Figure 26), only the shut-off valve that separates the liquids is actuated. Both liquids are pumped into their half of the reaction loop by a syringe pump until they meet on the other side. The outlet and the two inlet channels are then closed. Before the pump mechanism and thus the mixer is started, the shut-off valve must be opened again so that the two liquids can mix in a rotary movement. At the beginning, it could be assumed that the liquids will never mix, since laminar flow prevails in very small channels and the liquids are only pumped in a circle. However, if you look at the velocity profile within a channel, liquids move at a different rate close to the wall, which will be enhanced if the channel is circular. Also, the peristaltic movement stirs the two fluids when the membranes are actuated. For those reasons, mixing is possible with this

method. The pumping time until both samples are fused together is about 10 seconds at a pumping frequency of 50 Hz.

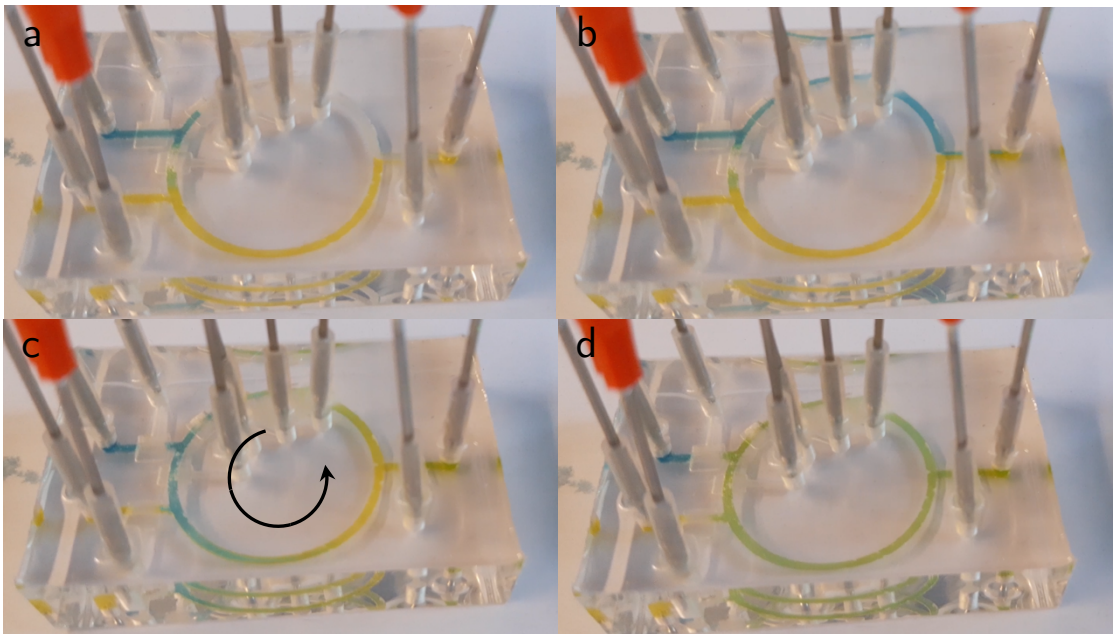

Figure 26: Course of the mixing process from (a) to (d). (c) shows the start of the rotation caused by the peristaltic pumping mechanism

5 Developing a microfluidic device for optical detection

Optical measurements for microfluidic applications are an essential tool for obtaining information from biological and chemical samples. Most of the optical processes associated with microfluidics are limited to laboratory use (off-chip detection), using conventional expensive microscopes. However, if these sensors can be incorporated directly into the microfluidic structure, on-site measurements can be carried out, which can deliver results in real time. Next to the advantage of portability, integrating these sensors would be beneficial for sensitivity as well. Techniques to measure optical behavior are absorbance, fluorescence and interferometer based techniques. Additional components for these measurements are light sources and micro lenses to improve detection. Detectors to measure the incoming light signal (electromagnetic waves) can be divided into photomultiplier tubes (PMT), charge-couple device sensors (CCD), Photodiodes and Complementary metal-oxide-semiconductor sensors (CMOS) [Bam07]. The rapid improvement in technology for developing electro-optical components and optical sensors enabled more powerful tools to be produced for lower costs. For this reason, expensive electro-optic components and evaluation systems are no longer reserved for large companies only [Tej19]. There are multiple fascinating techniques for optical detection, which won't be included in this thesis and can be reviewed elsewhere [Fra18]. Instead the focus lies on spectroscopy as one of the most important and influential analyzation methods and will be described in the following chapter. The goal is to show that a completely independent, integrated analysis system can be developed using the ESCARGOT method.

5.1 Spectral sensing

The Purpose of spectral sensing

In physics light is referred to as electromagnetic waves. Every object above 0 Kelvin is radiating electromagnetic waves, which can vary in wave length, amplitude, as well as intensity. The human eye can track wavelength in the range of 400 nm to 700 nm, known as the visible light spectrum. Besides the visible spectrum, the complete spectrum of light ranges far above and far below these wavelengths. In the field of spectroscopy, objects can be broken down into their elementary ingredients, by splitting them up into proportions of wavelength, energy and mass. Part of the field of spectroscopy is absorption spectroscopy, where the type and concentration of the emitted or absorbed radiation can be determined. Every material and every atom or molecule has characteristic, discrete energy levels. The electrons sit at these energy levels and can be raised to

a higher energy level when light is absorbed in the form of a photon. If a Material is placed between a spectrometer and a light source with a continuous spectrum, it absorbs photons of those energies that are given by the energy states of the material. The line spectrum then only reflects the unabsorbed light waves, as shown in Figure 27 below the continuous spectrum [Tip15] [Mes06]

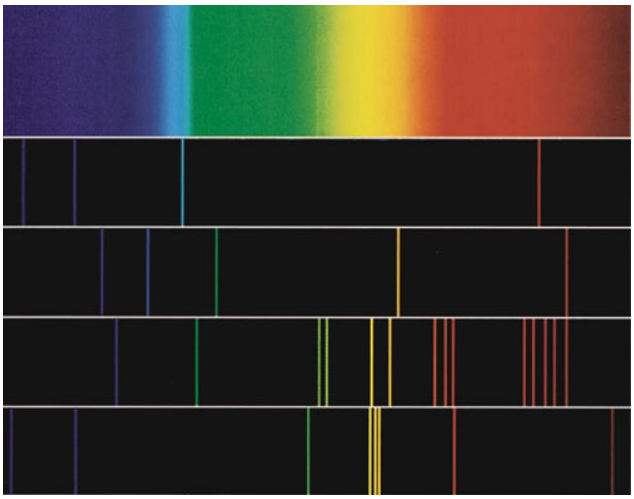

Figure 27: Above: A continuous spectrum in the visible range; below (from top to bottom) the line spectra of hydrogen, helium, barium and mercury. (© Eastman Kodak and Wabash Instrument Corporation.

Spectral sensing in Microfluidics

Optical measurements within the microfluidic scale can contain detections of elements, molecules, or other biochemical reactions and particles. Exemplary, absorption spectroscopy is commonly used to employ liquid chromatography, as proteins and nucleic acids strongly absorb UV light [Fra18]. However, there is a major setback on the microfluidic scale as sample volume decreases, sensitivity decreases as well, due to the short length of the optical path (Beer-Lambert law [Pop19]). In other words, this means a small signal to noise ratio for long optical paths and vice versa for small optical paths. This phenomenon can only be compensated if the optical elements are introduced into the microfluidic structure and as close as possible to the fluid channel and thus the sample [Rod16].

5.2 Spectral sensing PDMS device

When developing a spectral sensor prototype, different approaches can be chosen. In general, a sensor element is required that can measure the largest possible bandwidth of wavelengths, with the best possible resolution. For this purpose, the stimulating spectrum, i.e. the external light source, must reflect the entire wave spectrum as homogeneously as possible. To measure the absorption spectrum of a material, a reference spectrum must also be carried out under the same conditions. By combining the two measurements, the absorption spectrum of the material can be determined, as the spectrum of the sample is influenced solely by the experimental circumstances. This includes the material between the sensor and the sample, as well as reflections and light scattering from the light source. These must be compensated when evaluating the measured data. The sample-carrying channel should be as close as possible in front of the sensor lens to measure only the light emitted by the sample (fluorescence) and the light that is transmitted through the sample. The following chapters will present the development of a low cost, rapidly-made spectral sensing prototype in PDMS.

5.2.1 Materials

18-channel triad spectral sensor

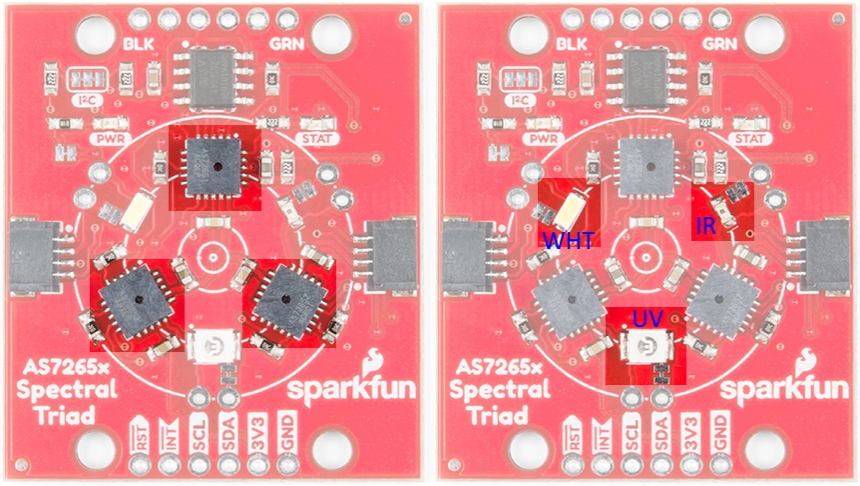

Figure 28: Left: AS72651 (UV), AS72652 (VIS), and AS72653 (NIR). Right: The Triad contains a 5700 k white LED, a 405 nm UV LED and a 875 nm IR LED [Spa20].

Figure 28 shows the spectral triad breakout board. The three sensors are highlighted on the left side of the picture. Each sensor can measure six wavelengths (Shown in Figure 29). On the right side three of the stimulation radiation sources are marked with WHT for a withe-light LED (5700k), IR for an infra-red LED (875 nm) and UV for an ultra violet LED (405 nm). The manufacturer chose these LEDs to illuminate the target with the largest swath of visible and invisible light. However, the stimulating spectrum coming from these light sources isn't homogeneous across the whole bandwidth, which is discussed in more detail in chapter 5.3.2. The LEDs can be individually enabled or disabled with software configurable drive current. [Spa20]

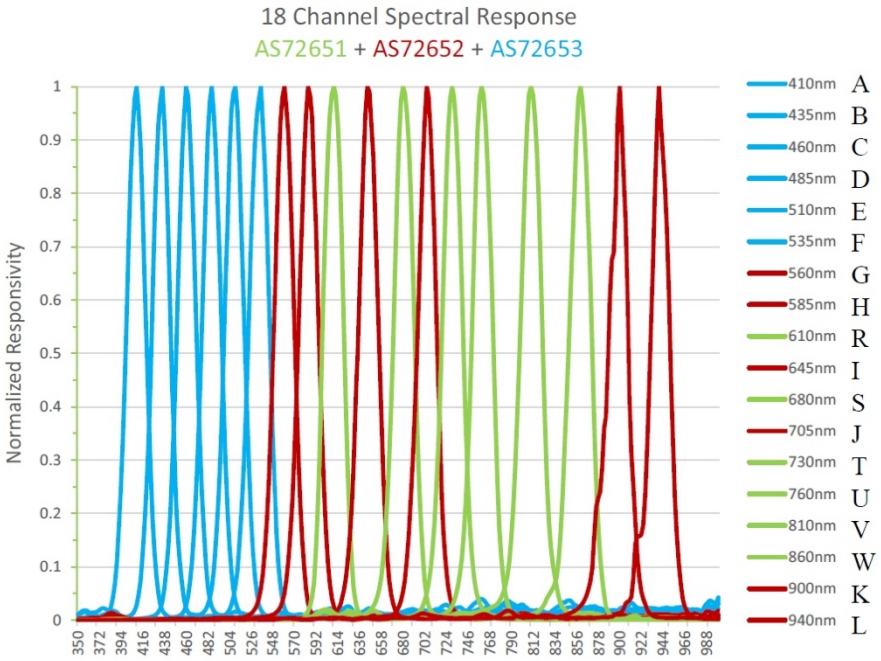

Figure 29: Normalized responsivity of all three spectral sensor units from the manufacturing datasheet. Each color reflects each measurable wavelength of each sensor [Spa20].

The communication between the sensor and the evaluation unit takes place via an I²C bus. The first sensor element AS72651 (the master) collects the data from the two other sensors AS72652 and AS72653 (the slaves) and forwards the combined data package to the evaluation unit. For this purpose, SparkFun Electronics[2] prepared a library to read out the data [Spa20]. Observing the spectral response graph (Figure 29), the normalized responsivity is plotted over the measured wavelength. Unlike a mass spectrometer, in which a continuous spectrum is measured, this sensor board has 18 discrete wavelengths

[2] SparkFun Electronics is an electronics manufacturer

with a resolution of ± 10nm. Each colour reflects each measurable wavelength of each sensor. The individual wavelength values are arranged on the right. The corresponding letters (A,B,C... etc.) are used for identification within the programming code.

The device family integrates Gaussian filters[3] into standard CMOS silicon via nano optic deposited interference filter technology in LGA[4] packages (Figure 30), that provide built-in apertures to control the light entering to the sensor array. Six of these filters are on each one of the sensors, whose spectral response is defined to its respective wavelength. The filters use an interference topology design which enables temperature stability with minimal drift over time or temperature. The triggering of the measurement is strongly dependent on the direction of light entry. As can be seen in Figure 30. The diffuse light can penetrate the sensor cover up to an angle of 20.5° (from midpoint) and is focused by the internal micro-lens onto the sensor chip.

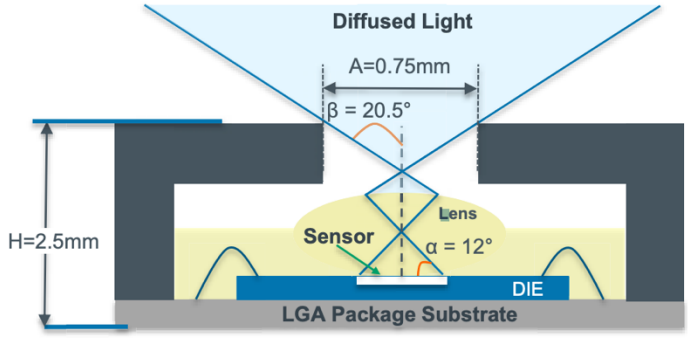

Figure 30: Schematic view of one of the sensor modules. Diffused light can be detected in an angle of ß=20.5°. A lens is focusing the light on the sensor chip [Spa20]

.

[3] Gaussian filters are used for noise-removing in electronical image pre-processing through pattern recognition [Has14]

[4] LGA are land grid arrays with a high density of contacts [Pcm20]

5.3 Developing a spectral sensing PDMS device

The PDMS device includes the triad 18-channel sensor and a microcontroller (Arduino Nano) as the processing unit. For illustration purposes, a colour display has been added to show the different wavelengths in form of a colored block diagram. Each block should represent a different wavelength, which is defined by its colour in respect to the continuous spectrum.

A schematic of the wiring of the components can be seen in Figure 31. Both the display as well as the sensor are communicating after one another over the I^2C bus. The driving voltage of the sensor board is 3.3V, while the display needs a supply voltage of 5V. Underneath the triad sensor board, a meander designed channel is placed for the spectral analyzation of the fluidic samples. Before PDMS is poured over the raw skeleton of electrical components, a fixture needs to be designed to hold everything in place.

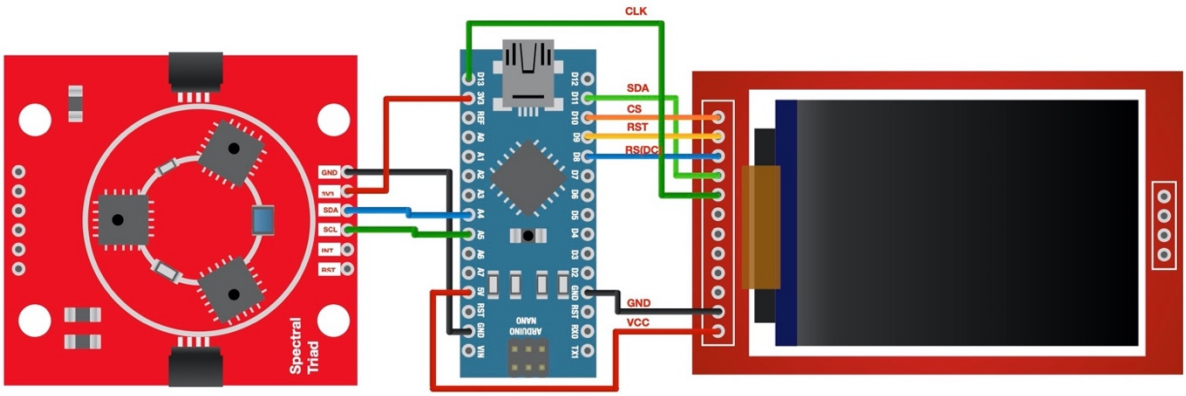

Figure 31: Wiring of the spectral sensor, the Arduino Nano and the colour display

A plain circuit board in the middle is connecting the Arduino Nano, the triad sensor and the display. Besides the display, all the other components and the connections between these components are soldiered to the circuit board, to ensure that there aren't any lose or moving parts as well as solid connections. The display will be plugged onto the board without soldering it, so that it can be removed before dissolving the ABS structure in Acetone. Acetone would attack the case of the display as well as the anti-reflective coating. Now that all the electronical components are soldered, they can be connected to the fixture with spacers. Above the triad sensor, the ABS channel will be placed and connected to the fixture with syringe needles. The completely assembled part is displayed in Figure 32 and is ready for the encapsulation process.

The ABS channel design (see orange structure on top of the sensor in Figure 32) was chosen so that it can be easily purged, as well as cover a big surface to absorb light coming from different angles if transmission is the desired method. If the on-board LEDs will be used the meander surface is also supposed to be reflecting as much light as possible.

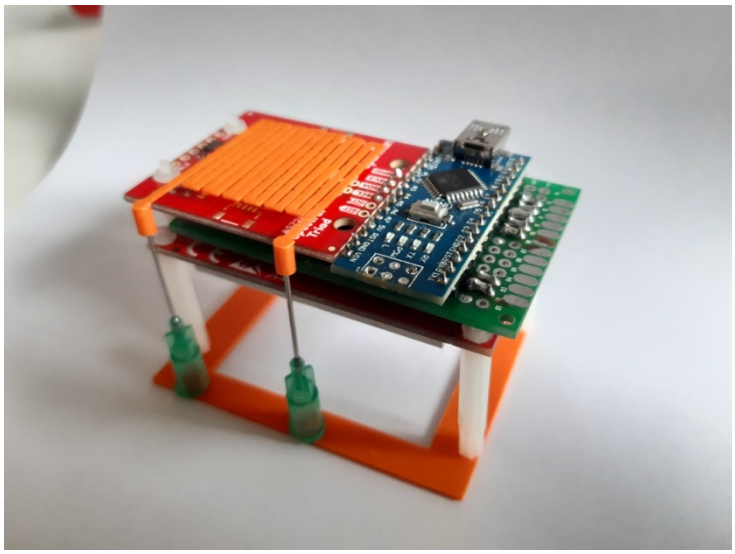

Figure 32: All components are ready to be poured with PDMS. To control the distance to one another, all components are connected to the same fixture.

5.3.1 Software

Sparkfun [Spa20] provides a variety of examples next to the downloadable library for controlling the sensor. Proving the concept of the sensor for detecting the spectral response data of fluids an example was chosen, which outputs the intensity of all 18-spectral wavelength. Next to the sensor code, the TFT display needs to be implemented. For this purpose, the Adafruit GFX library (Core graphics library) and the Adafruit ST7735 library for the displays driver IC need to be included in the code files. Every sensor data, so every intensity from 1 to 18 (representing the wavelength), is being mapped to a different color in the bar graph representing the spectrum of measurable light (Figure 29).

5.3.2 Testing the device and conducting measurements

To start the sensor module, it must be supplied with voltage via the USB connection as can be seen in Figure 33. This can be done either via a socket or a portable power bank. Changes to the functionality can only be made by rewriting the software code. The optical output takes place on the TFT display on the front of the component (Figure 34). The hose connections are directly below the display. To carry out a measurement, the sample can be introduced through one of the hose connections with a syringe. The sample must cover the entire sensor in order to carry out an accurate measurement. For the development of the prototype, the channel is visible on the bottom side within the PDMS, but should be shielded during an accurate measurement to avoid other light influences. The sample volume is ≈266µl.

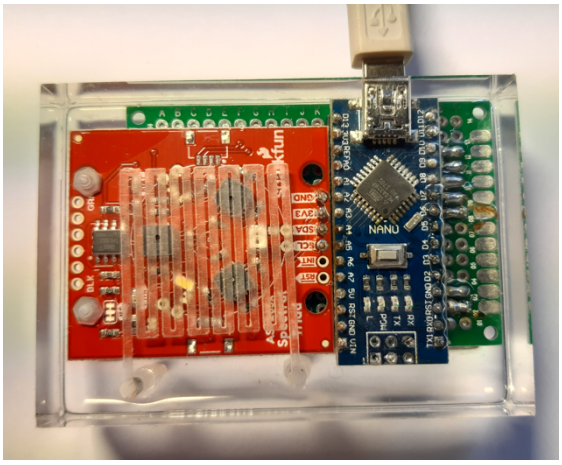

Figure 33: Backside view of the PDMS device

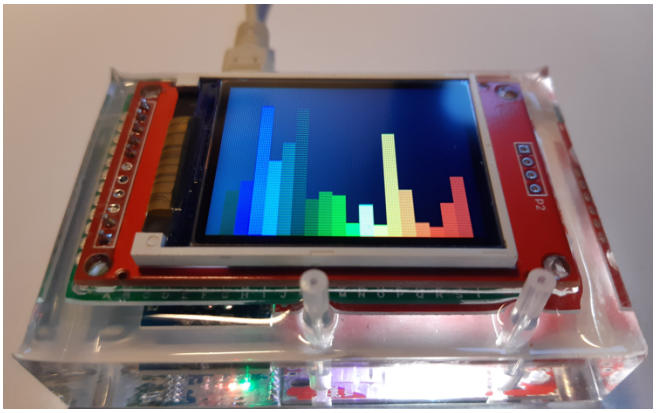

Figure 34: Front side view of the device. In- and outlet are at the lower side.

It is important to place the body on a black background to avoid other reflections. The stimulating light sources are on the sensor side and react with the sensors when the

emitted light is reflected on the sample, as well as by transmission through the sample when the emitted light is reflected on the surface below the component.

A proof of concept has been conducted using Rhodamine B solved in DI-water. Rhodamine B is a fluorescent dye with an emission-range of about 627 nm, when it is stimulated with a wavelength of 553 nm [Mer20]. A laser with a discrete wavelength of 532 nm was used to stimulate the sample. Figure 35 shows the normalized response graph. Intensity of all 18 wavelengths were measured with and without Rhodamine B. Normalization was achieved by calculating the percentage of gain. Values above 1 are reflecting enhanced light intensities when Rhodamine B is inside the channel. The normalized data drops at the point of the absorbed wavelength of about 535 nm, whereas a peak is reached at the wavelength of 610 nm representing the fluorescent emission.

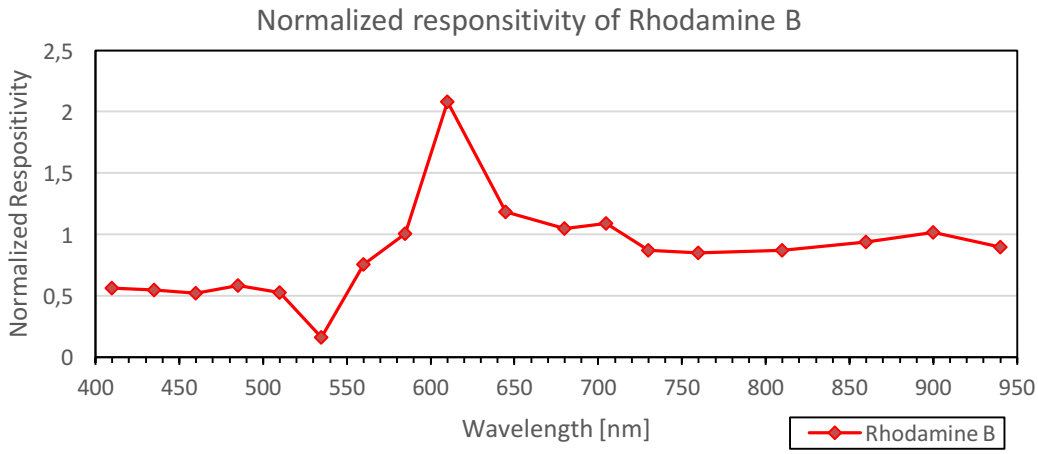

Figure 35: The graph represents the normalized responsivity of the measured emission of stimulated Rhodamine B

5.4 Conclusion and outlook

It could be successfully shown that it is possible to build a low cost, completely integrated PDMS device for measuring absorption spectra. The used sensor is not as powerful as a mass spectrometer, but it can give general indications which fluids are inside the fluidic chamber, as well as measure the intensity. Especially if the samples are tested and calibrated with the sensor beforehand. Measurements of Rhodamine B (the fluorescent dye) emissions could successfully be conducted, whereby the sample was stimulated through the discrete absorption wavelength.

Another method would be to use it as a pH-Indicator. For pH-Indicator measurement the sample, for example a cell culture, would need to contain pH indicator, such as phenol red [Atw14]. A changing color could therefore be measured in different wavelength that are emitted from the sample. Optical measurements and devices are still developed further and as more low cost and generally available devices and sensors arise, the easier it is to implement those in compact portable devices. The presented device is a first step to manufacture more specialized and portable solutions.

6 Developing a temperature controlling microfluidic device

In addition to the microfluidic modular components presented in the previous chapters, the heating of samples is of great importance in many chemical and biological processes, such as DNA amplification, cell culture and chemical reactions. How a temperature controlling PDMS device manufactured through the ESCARGOT method can yield many benefits and conduct different approaches compared to conventional methods will be shown through the following developing process. Many processes require a small deviation in temperature and stable temperature generation over time. A well-known example would be, the Polymerase Chain Reaction (PCR [Hou15]). A PCR is used in particular to detect viruses, such as the Coronavirus (COVID 19), which was influential worldwide in 2019 and 2020 [RKI20]. Figure 36 illustrates the sequences of a PCR analysis. Each step has a defined temperature range. As for the denaturation, a temperature around 94 °C to 96 °C is needed to split the double-stranded DNA templates. Followed by lowering the temperature at around 68°C for the annealing step to bind the DNA primer to the single DNA strings and subsequently increasing the temperature again (depends on the DNA polymerase used) for the elongation process. Each cycle doubles the DNA target sequence, leading to exponential growth [Zha07]. Transferring that to the temperature controller, means the more rapidly the heater reacts and regulates the target temperature, the faster the cycles can be carried out and thus less time is required for DNA amplification.

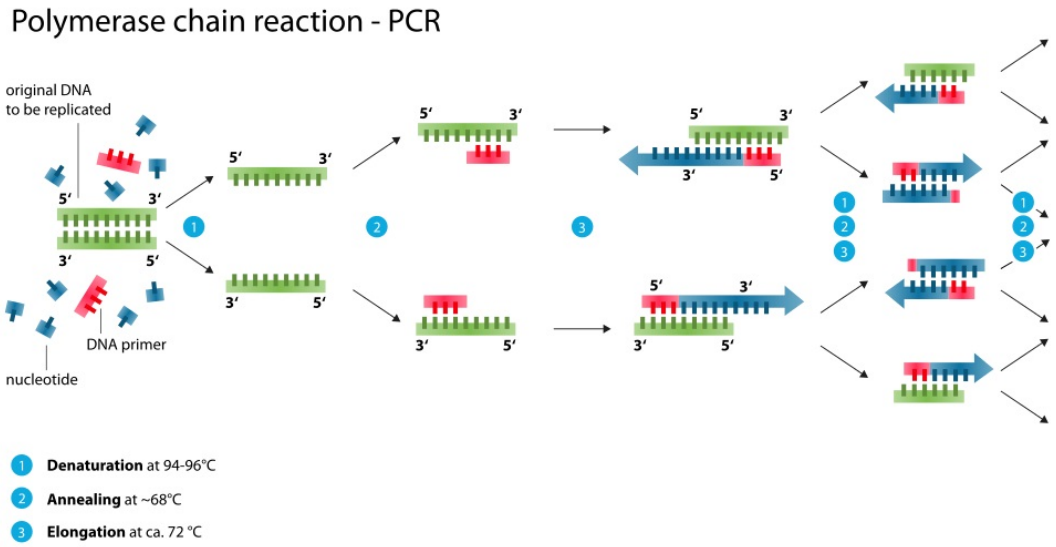

Figure 36: A PCR is a special case of application where precise and fast temperature control is important [Enz20].

A heated chamber can be developed using external heaters, integrated heaters or electromagnetic heating systems. Most heating systems on a microfluidic scale generate either a uniform temperature through the entire fluid or a temperature gradient. Which of these methods is suitable for a PDMS based device, is explained in the following section. In addition to selecting a suitable heater for the encapsulation process with PDMS, a suitable temperature sensor is also required to make the heating process controllable.

Before developing a temperature controller, there are a few challenges to keep in mind when designing such a device:

- How to heat the channel?
- Which material to choose as a heating element?
- How to measure the current temperature?
- How the surrounding material (PDMS) is affecting heat flow?
- How to implement the controller and evaluate the data?

6.1 How to heat a microfluidic channel.

External Heating includes the use of components such as Peltier elements to supply a previously heated liquid and inject it into the microsystem. The heated liquid doesn't represent the sample itself. It is used to transfer the heat into an opposite channel, where the target liquid resides [Mir13]. There needs to be a constant flow provided by a pump to compensate for the temperature loss. This is making the whole system less integrated and therefore less portable. Also, if no more liquid can be supplied trough the pumping system or in any other form, the device can't be heated anymore. For this reason, external heating is not suitable for a high integrated device, which in the best case should be portable.

Electromagnetic Heating is basically a different form of external heating, with the distinction that no heat transfer from one body or fluid to another fluid is necessary. The heat is generated within the fluid itself through exposure to long-wave microwaves [Mir13]. Depending on the materials used for the fluidic structures and substrate surfaces, only the fluidic channels are influenced by the prevailing electromagnetic field, which makes this method very selective. For this reason, the method offers not only the advantage of faster heating but also faster cooling [Wen20].

Integrated Heating can include a variety of methods. An example similar to the external heater would be to add heating channels as before next to the channel which

need to be heated. This time the heat is not supplied from the outside, but coming from the reaction of two different reagents that can either heat or cool the channel next to them [Mir13]. A simpler method would be to use a resistance wire. A resistance wire is usually used to limit the amount of current in a circuit. As a usually unwanted side effect, the wire warms up as a result of the current flow. The higher the resistance of the wire, the more voltage it drops. More voltage drop means a higher loss of power and therefore a higher temperature output. For this reason, the wire should be very stable in high temperatures so that it does not burn through like a fuse. With the encapsulation process for manufacturing PDMS devices (ESCARGOT) the resistance wire could be placed directly next to the channel or wrapped around like a coil. Leaving a small gab between the wire and the channel will prevent the wire from getting in contact with the fluid sample. The gab should be small enough to have virtually no temperature gradient and therefore less loss of heat to the surrounding area.

6.2 Choosing a suitable wire material

The process to heat a resistive wire is called Joule heating [Mir13]. Here, the flow of electrical current through a wire generates thermal energy. Choosing a wire material has an impact on the amount of electrical power to be applied as well as on the size or length of the wire to be implemented. Another factor is the resistance itself, as resistor materials tend to change their resistance when an electrical current is applied. For a positive temperature coefficient of electric resistivity, the resistances value would therefore increase, which would result in a higher current consumption. A low temperature coefficient would be advisable to minimize this effect. The mechanical properties of such a heating wire is another key attribute. The better it can be deformed, the better it can be adapted to the shape of the channel or the heating chamber. If it's too soft, it could be more difficult to stabilize and to keep it in the required shape, as it is deforming on its own weight.

With little research the main material, for almost every heating application involving resistive heating, are nickel-chrome alloys (nichromes) [The11]. Nichrome wires fulfil all the desired characteristics and properties from above. The resistance of a nichrome wire changes very little with temperature. Its resistance only increases by 7 % when changing from 20 °C to 400 °C; and only increases another 1 % from 400 °C to 1000 °C. The temperature coefficient of resistance of nichrome is much lower than that of most common metals. They can also withstand temperatures of up to 1200 °C, which is more

than enough for most microfluidic applications [Res20]. The relationship between resistance and temperature coefficient for calculating the temperature change, can be calculated using the following formula.

Relationship between resistance & temperature:

$$R = R_{ref}[1 + \alpha(T - T_{ref})] \quad 6.1$$

$$T = T_{ref} \frac{(R - R_{ref})}{(R_{ref} * \alpha)} \quad 6.2$$

R = Conductor resistance at temperature "T"
R_{ref} = Conductor resistance at reference temperature T_{ref}, usually RT
α = Temperature coefficient of resistance for conducor material
T = Conductor temperature in degrees Celcius
T_{ref} = Reference temperature that α is specified at for the conductor material
$\alpha_{NiCr} = 0.0004\ {}^{1}/_{\circ C}$ [Res20]

The temperature coefficient for nichrome is really small, which indicated a low deviation of resistance for creating higher temperatures.

6.3 How to measure the temperature.

There are two options to measure the temperature. It can either be measured through a sensing unit or calculated by the temperature gradient from the generated heat by the nichrome wire [Yan14]. The sensor unit can be further divided into invasive, semi-invasive and non-invasive techniques. Thermocouples, resistive thermometers and thermistors can measure the temperature through direct contact (invasive) as well as non-invasive (calculating the actual channel temp through temperature gradient). Methods like infrared thermography are completely non-invasive, while thermochromic liquid crystals (TLCs) or temperature sensitive fluorescent dyes such as rhodamine B are semi-invasive and measure the temperature indirect [Yan14]. Direct invasive measurements can only take measurements at certain placement points and add their thermal mass to the measurement system, whereas non-invasive and semi-invasive optical measurements observe the entire channel.

6.4 Choosing a temperature sensor

Before choosing between the listed technologies for temperature measurements inside a microfluidic channel, optical thermography can be excluded in advance. These methods are not suitable for an automated controlling device, due to their low accuracy [Fan18]. Integrating them into the temperature control device would create significant challenges, since optical measurements would need specifically made evaluation units that could produce a measurement output for the controller to compute. Next to the fact that infrared thermography instruments are one of the more expensive measurement technologies. TLCs have a narrow temperature range and limited spatial resolution as well as TLCs and temperature-sensitive fluorescent dyes would change the composition of the sample by the potential for unintended reactivity with the processing reagents. For this reason, they cannot be used for all temperature applications. Leaving the list of direct measurements to choose from. Thermocouples are one of the most common temperature measurement types and employ the Seebeck effect[5] of thermoelectric materials. Because it's really cheap compared to other methods and also its reliability, thermocouples have already been used in a variety of temperature sensing applications. Compared to resistive temperature detectors, commercially available thermocouples have a lower temperature resolution [Ome20]. Additionally, RTD[6]s are easier to miniaturize and implement into the microstructures. Another temperature sensor is a thermistor. Thermistors are closely related to RTDs with the difference that the sensing element of thermistors are ceramic or polymer resistors instead of metal. Unlike thermistors, resistive temperature detectors have an extremely linear output, producing very accurate measurements of temperature. Making thermistors unstable over long periods of time. All these factors contribute to the decision of choosing a resistive temperature detector inside the fluidic channel.

[5] The Seebeck effect is a thermoelectric effect, where electric potential can be measured between two different wires which are made from two different materials. When the end of these wires are connected which each other (like iron and copper) and a temperature can be measured at the connection point. The other end of the wires must be maintained in a constant reference temperature environment. The potential difference is proportional to the temperature difference. [Bul08]

[6] Resistance temperature detector (RTD) are usually thin film resistance structures out of platinum used for temperature measurements [Jik01].

6.5 How to control the temperature.

A fast-operating temperature controller will respond rapidly to changes, whether due to internal or external influences. In addition, to reduce the time to reach the desired target temperature, many processes are dependent on small temperature deviations as well as avoiding excessive surges. These prerequisites would be decisive for processes like a PCR. To fulfil the mentioned requirements, a PID controller is particularly suitable, which not only reacts quickly to changes due to the D part but is also fairly accurate due to the I part.

PID Control

A PID controller is a three-term controller with a proportional (P), integral (I) and differential (D) quantity. The controller is part of a feedback control loop. The desired signal value is the incoming setpoint at the loop entrance. Compared to the current signal value, the controller calculates the offset between these two and sets a correction factor/ error to regulate the actuator accordingly to reach the setpoint value. [Rak20]

In a PID controller the controller output is calculated in three different algorithms. Each of these algorithms has its own tuning parameter Kp, Ki & Kd which can be adjusted manually to reach the desired performance. Combining P and I controller is enough to establish an accurate control loop for most applications. Though, adding a derivative algorithm to the equation can allow for bigger P and I gain, while still keeping the loop stable. In other words, this will result in a faster response and better performance.

6.6 Developing a PID controlling PDMS device

Every process that demands a stable regulated temperature, controllers are needed. Temperature can be varied via actively heating or cooling the system to attain the specified setpoint (target temperature). The last chapter described the functionality of a PID-controller, which will be used in the following prototype device. Next, the chosen heating wire, as well as the temperature sensor will be presented.

6.6.1 Materials

In the previous chapters, various options for heating microfluidic channels and for measuring the temperature inside those were explained and discussed. Appropriate methods could therefore be selected. Finally, the task is to look for suitable components from the knowledge gained.

Nichrome Wire

Nichrome (NiCr) is a metal alloy consisting of primarily nickel and chromium. Varieties of NiCr are available with different proportions of nickel and chromium as well as small amounts of other elements. The more common varieties are nichrome-80 (most common) and nichrome-60 which are approximately 80% and 60% nickel, respectively. Both varieties have maximum operating temperatures of about 1100°C – 1200°C and melting temperatures above 1400°C [Hea20]. The chromium will form an oxide layer on the wire's surface which protects the wire from corrosion. The corrosion resistance, the high melting temperature, and a higher resistivity than many other metals make NiCr a good material for electrical heating elements. A wire with a diameter of 100 µm was chosen, due to its ease in adaptability. The chosen wire has a resistance of 153,8 Ohms/m.

6.6.2 Simulation

Needed parameter for thermal analysis:

Sylgard 182 Dow Site[7]:

- Thermal Conductivity 0.16 W/K*m
- Density 965 kg/m^3

Nichrome wire[8]:

- Thermal Conductivity 11.3 W/m*°C
- Density 8400 kg/m^3

The simulation was conducted to investigate the temperature behavior inside the fluidic channel where the sample resides. To heat the channel to the desired temperature, the heating coil needs to be as close as possible to reduce the temperature gradient. A greater distance, the higher the temperature loss between coil and fluid. That results in a higher temperature of the heating coil itself. The higher the temperature of the heating coil the more easily the surrounding PDMS could be effected and damaged. To exanimate the temperature gradient the behavior of water inside the fluid channel was simulated applying a value of 100 °C to the nichrome coil, as can be seen in Figure 37. Due to temperature loss at the cross-section of the PDMS layer between the fluid and the

[7] Values for PDMS crosslinked and cured at room temperature for 48h

[8] NichromeWire d=0.095 AWG38 Ni80 Cr20

heating coil, the fluid temperature results in 95.85 °C. This temperature loss is considerably low since PDMS is operational up to temperatures of 200 °C [DOW20]. Implying that the channel can be heated to temperature close to 200 °C.

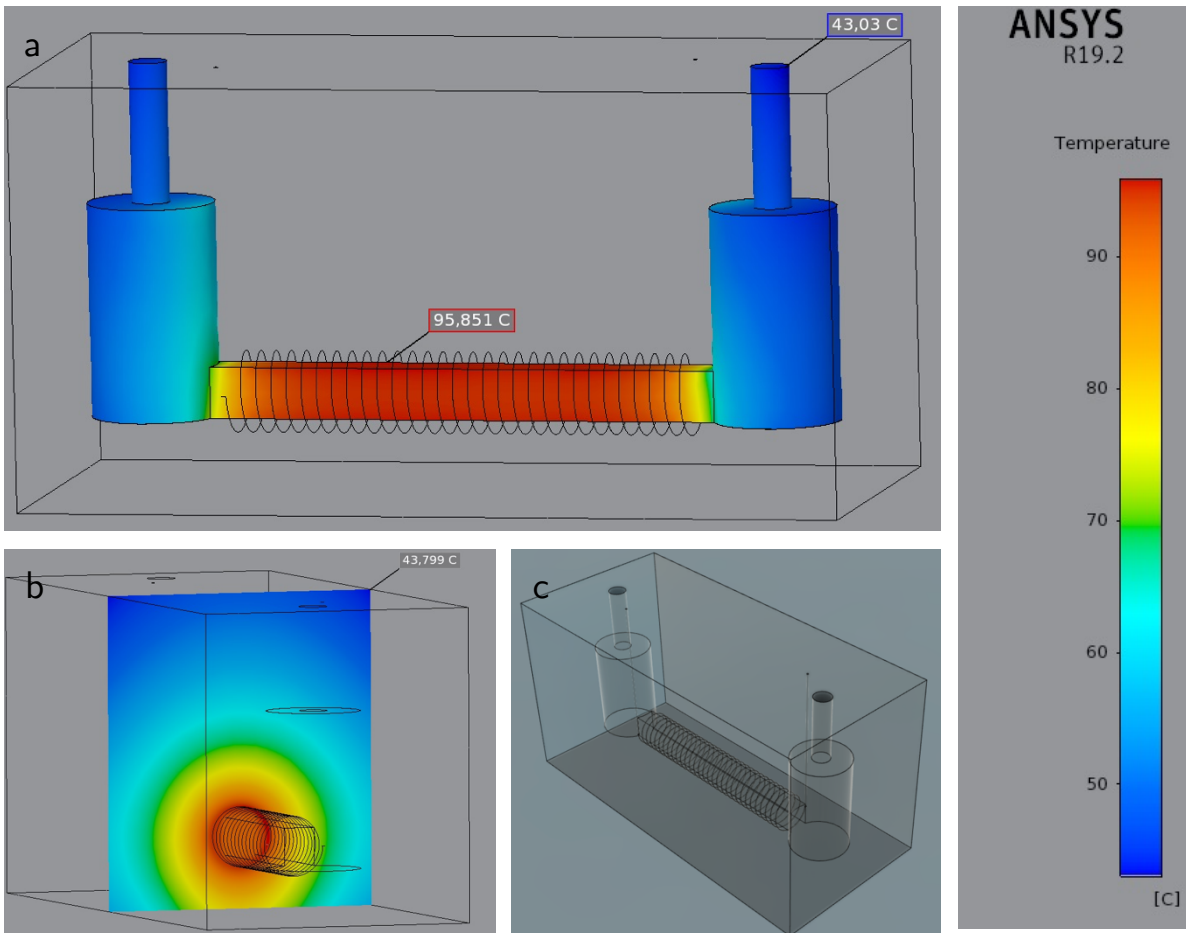

Figure 37: The Simulation was conducted in Ansys Aim 19.2v. (a) shows the channel to be heated. The surrounding black coil represents the nichrome wire with a temperature of 100 °C. (b) Cross-sectional profile of the simulated body. The Outside of the PDMS device has a temperature of approximately 43.8 °C. (c) The design of the simulated device. The channel is surrounded with the nichrome wire in the middle. In and outlets, can be seen on the top of the model.

PT1000

The chosen PT is a simple resistance temperature detector (RTD) using a platinum resistor in thin film technology as a sensing element. The characteristic curve of this Platinum RTD complies with DIN EN 60751 [Tec20]. Another reason choosing it for temperature measurement inside a microfluidic channel, is its small outline dimensions. The ceramics substrate on which the platinum film is structured on as well as the glass coating make the sensing element chemically inert and therefore protect the fluid samples.

The calculation formulas of Pt-RTDs are defined in DIN EN 60751 as following [Tec20]:

$$R_{(T)} = R_{(0)}(1 + a * T + b * T^2)$$

With the coefficients given:

$$a = 3.9083 * 10^{-3}$$

$$b = -5.775 * 10^{-7}$$

Resulting in an almost linear behavior due to a very small b value.

6.6.3 How to read out the data.

If the PT1000 would be connected to an Arduino directly, the readings of the temperature measurement would be limited by the resolution of the 10-bit analog to digital converter. 10-Bit means $2^{10} = 1024\,units$. While RTDs like the PT1000 are highly accurate, they have very poor thermal sensitivity (around 1 Ω/°C), that means a change in temperature produces a very small output change. There are specially made solutions to amplify the signal of a PT1000 like the MAX31865 IC[9] (Figure 38).

While the picture shows the complete breakout board for the MAX31865 from Adafruit, the 15-Bit ADC is on the main chip in the middle of the board. The resolution in temperature is given with 0.03125 °C in the manufacturing datasheet [Max20]. That is more than enough considering the PT-Sensor itself yields a resolution of ±0.1 °C. Every component should be chosen carefully, as they define the final size and form of the PDMS device.

[9] IC = integrated circuit. ICs can combine a variety of electrical functions in one component.

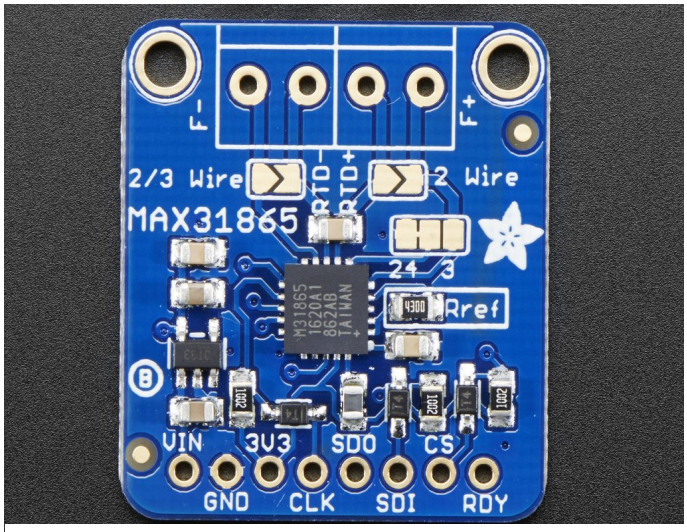

Figure 38: The MAX31865 is a signal amplifier IC. mounted on the Adafruit breakout board.

6.7 Manufacturing the PID PDMS device

Before encapsulating the components in PDMS, the functionality of the system has been tested surrounded by air. Bringing the NiCr wire close to the PT sensor is enough to measure and control the temperature to its desired value. After proving the functionality of the system, the PT1000 with its signal amplifier, the ABS channel and the heating coil were enclosed in PDMS. To be able to interface the device wires, connectors, as well as hose connectors for the fluid, are on the outside of the prototype.

Important is the resistivity of the wire coating against Acetone. Common wire enclosures dissolve in the ABS removal process and need to be changed to silicon coated wires.

Figure 39 shows the basic prototype. The fluidic channel is barely visible and can be detected by the NiCr wire strapped around its surface. While the wire isn't touching the fluid due to the surrounding PDMS, no temperature gradient needs to be calculated since the temperature measurement is happening inside the channel. The yellow wires connect the MOS-Module with the heating element and are soldered to the NiCr wire. At the other end of the device are the interfacing pins. The MAX31865 breakout board needs to be powered with a voltage between $3 - 5$ VDC. All other Pins are for the SPI-communication with the Arduino.

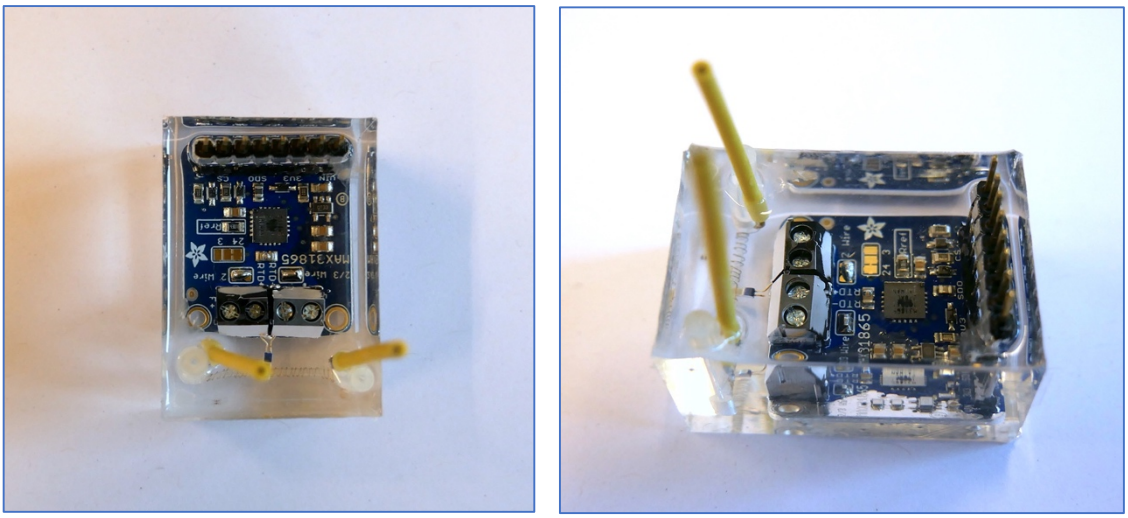

Figure 39: Left side shows the top view of the PID prototype. Right side shows a top side view. On both pictures the channel is barely visible only by following the NiCr wire wrapped around the structure. The main Part of the

Software

The Arduino code for this device consists mainly from the Adafruit_MAX31865 library to measure the current temperature and the PID_v1 library from Brett Beauregard [Bre20] for the temperature control.

6.7.1 Operation principle and measurements

Figure 40 displays the wiring of the PDMS device with the MOS-module as well as the Arduino. The Arduino receives the current temperature value through the amplifier data port SDO. This incoming value is being processed by the software PID control, which outputs a PWM[10] Signal [Ger11]. With each step defined by the sample time, a new output and therefor a PWM signal is being calculated and send to the MOS module.

[10] PWM is a signal modulated by its pulse width

Considering that the Arduino can only output 40 mA, the outgoing signal would be too weak to generate temperatures above 50 °C powering the NiCr-wire. The mentioned MOS-module solves this problem. The incoming PWM-Signal switches a much heavier power supply. As a result, the MOS module is emitting the same PWM Signal with a higher amplitude and therefore generating the desired heat. A heavier power supply could be a 9 V battery as shown in Figure 40.

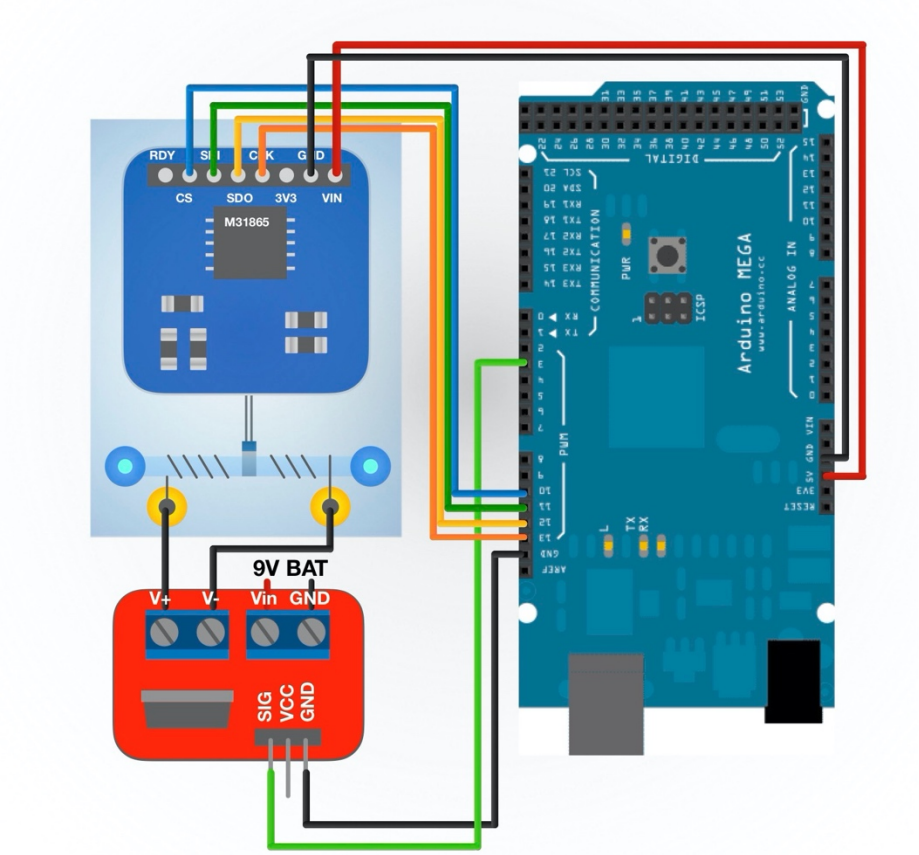

Figure 40: Wiring of the components. Top left shows the PDMS device consisting of the PT-Sensor, the fluid channel, the NiCr-wire and the MAX31865 amplifier. Below the PDMS device is the MOS-module as an PWM interface between the Arduino and the PDMS device.

PID measurements:

Test recordings of the controller were taken and plotted to demonstrate the functionality. For that standard gain values for Kp, Ki, and Kd were chosen. Distilled water was used as an example material. To optimize the controller behavior different gain values could be chosen, creating a faster and more accurate response. Measurements have shown a successful attempt to control a temperature of 60 °C ±0.25°C shown in the first graph Figure 41. Although the used parameters produced a relatively long wait time of about 2 minutes, for the channel temperature to reach the desired temperature (Setpoint).

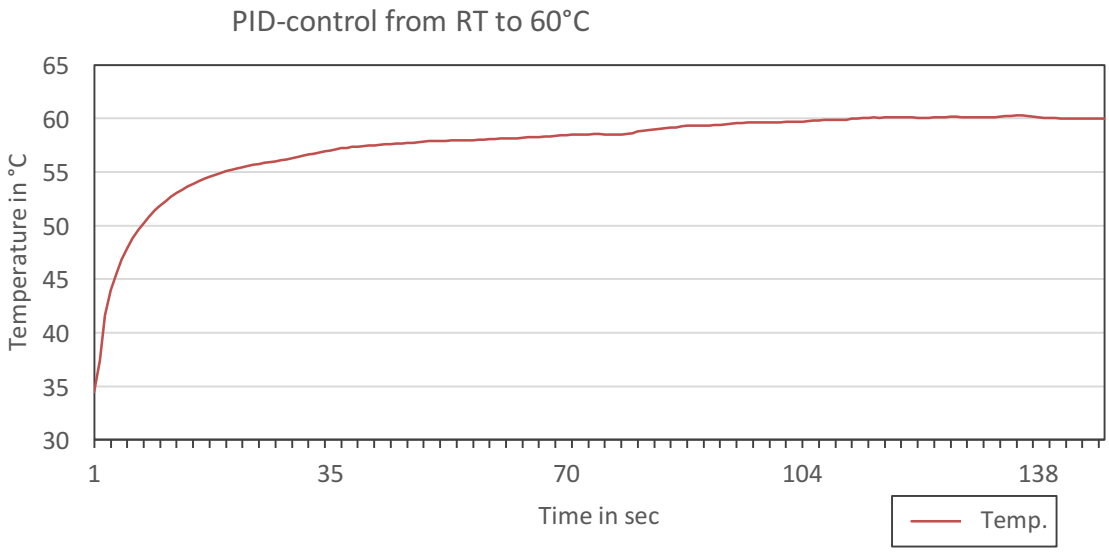

Figure 41: Temperature measurement inside the channel. The Setpoint is set to 60°C which will be reached at approximately 2 minutes.

A different behavior with different gain factors could be shown for the regulation at 80 °C. If the proportional gain factor (Kp) is too high, the value of the channel temperature will always oscillate around the setpoint. This means that if the proportional gain is too high, the temperature value briefly exceeds the setpoint. Consequently, temperatures in the channel can exceed 80 °C. At temperatures of 90 °C to 100 °C, water vapor bubbles can be generated within the channel. When these steam bubbles move over the sensor due to the movement of heat, there is a direct temperature loss at the sensor. The PID controller wants to counteract this loss and regulates it more strongly than before, which again causes a sharp rise in temperature. If the sensor is wetted again due to the constant movement of water, the measured temperature rises rapidly and the controller regulates back significantly. This constant back and forth created by the water

vapor bubbles. This phenomenon is shown in graph in Figure 42. As soon as the temperature rises from 60 °C to 80 °C, the system begins to oscillate. If we then set the setpoint back to 60 °C, the oscillation stops

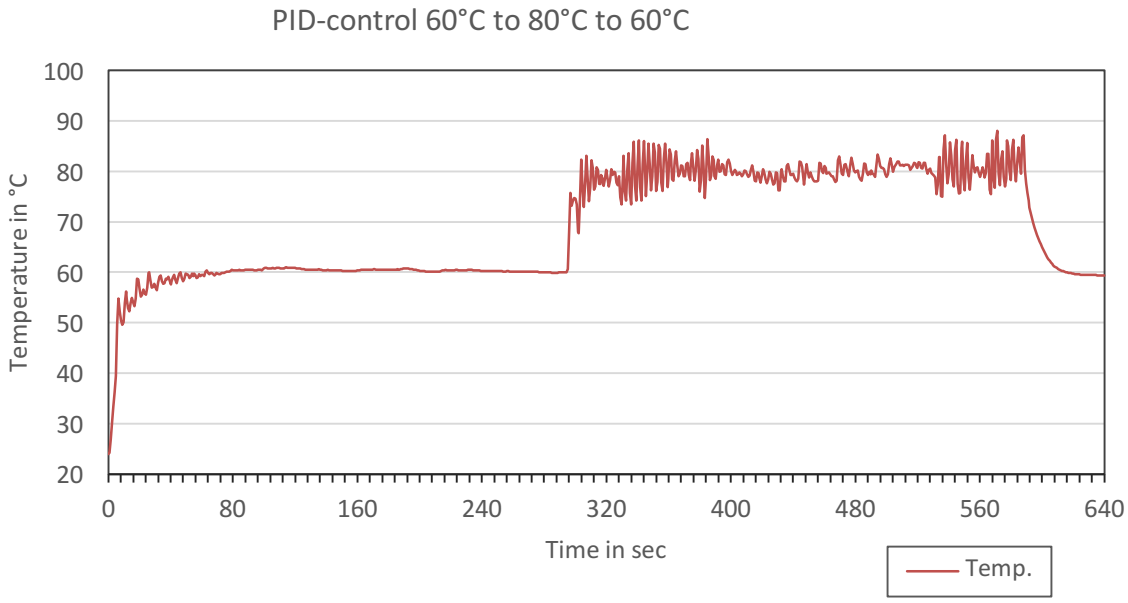

Figure 42: Temperature measurement inside the channel. The Setpoint changes after every 300 seconds from 60°C to 80°C and back to 60°C.

6.8 Conclusion

Conclusively, a PID controlling PDMS device could be successfully developed. The embedded scaffold method has the capability to directly embed the temperature sensor inside the flow channel. That way the measurement doesn't need to be calculated/ calibrated if the sensor would be near the channel. Another benefit is the short wire distance if the attached component, such as the measurement signal amplifier as well as a micro-computer are embedded in PDMS as well.

There remain open solutions to optimize the application, for example by finding suitable Kp, Ki, and Kd values, as well as optimizing the control at values at which the liquid begins to evaporate. Local evaporations must be prevented in order to generate a temperature close to the evaporation temperature. Other optimizations include the composition and structure of the entire device to adapt it to its respective applications.

Future measurements and tests can also involve the execution of a PCR, which would also benefit from a combination of the temperature controller with optical sensors to directly measure fluorescence behavior of the sample.

7 Conclusion and outlook

The thesis investigated the possibility to develop integrable modular microfluidic structures and combining those with electrical components. The presented ESCARGOT method [SV15] was successfully used to develop multilayer structures enclosed in PDMS, to directly interconnect electrical sensors and heating elements within the fluidic structure, as well as establish active microfluidic components. These active fluidic elements like quake valves could be incorporated into a PDMS bulk using prototype alignment techniques, to subsequently generate fluidic logic gates. By arranging these active fluidic valves in series, a peristaltic pumping mechanism could be developed. Through further integration, this pumping mechanism was used to develop a fluid mixer and a droplet generator as well. The functionality of these components was tested and compared with existing scientific work, showing similar results in functionality. However, the method presented in comparison to other developing technologies shows low fabrication costs and short production times, due to the 3D printing technology and the scaffold removal process. Developing the alignment between the components further can increase the reproducibility of the components, as well as increase the general complexity. Next to the developed quake valves, different valve mechanisms should be conducted in the future, which have a low energy consumption and could be incorporated inside the device. That could contribute in developing portable devices, without the reliance on external controlling units. Investigating functional portable microfluidic devices is an important subject for the future.

To show how complex prototypes can be developed from modular fluidic and electronic components, an 18-channel spectral detection device and a temperature-controlling PID device were constructed. The spectral sensing device, is a fully functional spectral sensor combined with a processing unit and a fluidic channel below the sensor and can output the measured data immediately on the attached display. Basic fluorescents measurements with Rhodamine B were successfully conducted and presented. Further tests can investigate the behavior under different conditions with different fluids. Generally, it is good for prototyping to see the incorporated materials and sensors, as well as having visual feedback of the fluid. However, for spectral or optical analysis it would be advised to manufacture a cover, so that no other light sources affect the measurement. Additionally, to developing the fluidic structure, PCBs could be developed as well to directly fit the sensors and other electrical components in a suitable layout, before enclosing them inside the PDMS body.

The PID temperature controlling device could regulate the temperature to the target temperature through the use of a 9V block battery. Making the whole system portable and ready for on-site measurements. However, the temperature control has to be optimized in order to generate a small control deviation even at temperatures around the boiling point. Afterwards first attempts at PCR analysis could be carried out in the near future. Developing additional prototypes, which combine optical sensors directly with temperature control could detect the success if the PCR directly within the prototype.

Next to the presented method of 3D printing, different technologies for structuring the ABS scaffold should be tested in the near future. Nevertheless, it can be assumed that the upcoming 3D printers will be able to print in ever higher resolutions. In addition, more and more exotic filaments are being developed which could offer new possibilities for the development of microfluidic structures and components. Much can be expected from the 3D printing technology in the future, as production costs decrease for custom device manufacturing as well as scaling-up or scaling-down for 3d designs is a straightforward process.

8 References

[Abi19] Abigail K. Grosskopf, Ryan L. Truby, Hyoungsoo Kim, Antonio Perazzo, Jennifer A. Lewis, Howard A. Stone. *Viscoplastic Matrix Materials for Embedded 3D Printing.* (2018)

[Adi20] Aditi Naik, Yiliang Zhou. *Microfluidic Valves.* www.openwetware.org/wiki/Microfluidic_Valves_-_Aditi_Naik,_Yiliang_Zhou (28.11.2020)

[All20] All3DP *The Types of 3D Printing Technology in 2020* https://all3dp.com/1/types-of-3d-printers-3d-printing-technology/ (26.11.2020)

[Att09] Attia, U.M., Marson, S. & Alcock, J.R. *Micro-injection moulding of polymer microfluidic devices.* Microfluid Nanofluid **7,** 1 (2009).

[Atw14] Atwe, A. Gupta, R. Kant, M. Das, I. Sharma, S. Bhattacharya. *A novel microfluidic switch for pH control using Chitosan based hydrogels.* Microsystem Technologies, 20:1373-1381. (2014)

[Bam07] Bambang Kuswandia, Nurimana, Jurriaan Huskensb, Willem Verboom. *Optical sensing systems for microfluidic devices: A review.* Elsevier B.V. All rights reserved. (2007)

[Bec00] Becker H., Heim U. *Hot embossing as a method for the fabrication of polymer high aspect ratio structures.* Sensors and Actuators A: Physical, Volume 83, Issues 1–3, Pages 130-135 (2000)

[Bel00] Belorgey G., Sauvet G. *Silicon-Containing Polymers: The Science and Technology of Their Synthesis and Applications.* Kulwer Academic (2000).

[Bre20] Brett Beauregard. *Arduino PID Library.* https://playground.arduino.cc/Code/PIDLibrary/ (28.11.2020)

[Bro20] Brosseau A., Brouillard A. *Pneumatic valves.* https://openwetware.org/wiki/Pneumatic_Valves_-_Alex_Brosseau,_Anthony_Brouillard (28.11.2020)

[Bul08] Bulusua, D.G. Walkerb. *Review of electronic transport models for thermoelectric materials*. Science Direct Superlattices and Microstructures 44 1–36 (2008).

[Chu05] Chung-Cheng Lee, Guodong Sui, Arkadij Elizarov, Chengyi Jenny Shu, Young-Shik Shin, Alek N. Dooley. *Multistep Synthesis of a Radiolabeled Imaging Probe Using Integrated Microfluidics.* Science Vol. 310, Issue 5755 (2005)

[Cip12] Ciprian Iliescu, Hayden Taylor, Marioara Avram, Jianmin Miao, and Sami Franssila. *A practical guide for the fabrication of microfluidic devices using glass and silicon.* Published Online: 05 March 2012, (2012).

[DOW20] DOW. *SYLGARD™ 184 Silicone Elastomer Kit Technical Data Sheet.* https://www.dow.com/ (28.11.2020)

[Emm16] Emmanuel Roy, Antoine Pallandre, Bacem Zribi, Marie-Charlotte Horny, *Overview of Materials for Microfluidic Applications.* Article published November (2016)

[Eve20] Eveflow. *Materials for microfluidic device fabrication: a review.* www.elveflow.com/microfluidic-reviews/general-microfluidics/materials-for-microfluidic-chips-fabrication-a-review-2017/ (27 November 2020)

[Enz20] Enzoklop, https://commons.wikimedia.org/wiki/File:Polymerase_chain_reaction.svg CC BY-SA 3.0 <https://creativecommons.org/licenses/by-sa/3.0>, via Wikimedia Commons (29.11.2020)

[Fan18] Fan Yang, Nana Yang, Xiaoye Huo, Shengyong Xu. *Thermal sensing in fluid at the micro-nano-scales.* Biomicrofluidics. Jul; 12(4): 041501. (2018)

[Fra18] Frank B. Myers, Luke P. Lee. *Innovations in optical microfluidic technologies for point-of-care diagnostics***.** Lab on a Chip, Issue 12 (2018)

[Fre17] Freedman Jeri. *Future Uses and Possibilities of 3D Printing.* Cavendish Square Publishing, LLC, (2017)

[Ger11] Gerald Recktenwald. Basic Pulse Width Modulation. EAS 199: https://cdn.sparkfun.com/assets/resources/4/4/PWM_output_Arduino.pdf November 14, (2011)

[Gri20] Grieser Franz. *What resolution can 3D printers print?* https://all3dp.com/3d-printer-resolution/ (26.11.2020)

[Gui20] Guilhem Velvé Casquillas and Timothée Houssin. *PDMS: a review* www.elveflow.com/microfluidic-reviews/general-microfluidics/the-poly-dimethyl-siloxane-pdms-and-microfluidics-2/ (23 November 2020)

[Has14] Hassene Seddik. *A new family of Gaussian filters with adaptive lobe location and smoothing strength for efficient image restoration.* EURASIP Journal on Advances in Signal Processing volume 2014, Article number: 25 (2014)

[Hea20] Heating-element-alloy. *NiChrome Alloys for Heating Applications.* https://www.heating-element-alloy.com/article/nickel-alloys-for-heating.html (29.11.2020)

[Her19] Hernández Vera, R., O'Callaghan, P., Fatsis-Kavalopoulos, N. *et al. Modular microfluidic systems cast from 3D-printed molds for imaging leukocyte adherence to differentially treated endothelial cultures. Sci Rep* **9,** 11321 (2019).

[Hou15] Timothée Houssin Microfluidic *PCR, qPCR, RT-PCR & qRT-PCR* www.elveflow.com/microfluidic-reviews/general-microfluidics/microfluidic-pcr-qpcr-rtpcr/ (June 2015).

[Hyu09] Hyungsub Choi, Cyrus C.M. Mody. *The Long History of Molecular* Electronics: Microelectronics Origins of Nanotechnology. Sage journals, Volume: 39 issue: 1, page(s): 11-50. (2009).

[Imr07] Imran Fazal. Development of gas microvalve based on fine- and micromachining. PhD. Thesis, University of Twente, the Netherlands (2007)

[ISO16] ISO. *ISO 7864:2016 Sterile hypodermic needles for single use* ICS :11.040.25 Syringes, needles and catheters (2016)

[Jac05] Jacques Goulpeau. *Experimental study and modeling of polydimethylsiloxane peristaltic micropumps.* Journal of Applied Physics 98, 044914 (2005).

[Jae10] Jaeger Richard C. *Microelectronic circuit design.* Published by McGraw-Hill 4th ed. (2010)

[Jer10] Jeremy J. Agresti, Eugene Antipov, Adam R. Abate, Keunho Ahn, Amy C. Rowat, Jean-Christophe Baret, Manuel Marquez, Alexander M. Klibanov, Andrew D. Griffiths, and David A. Weitz. *Ultrahigh-throughput screening in drop-based microfluidics for directed evolution.* PNAS March 2, 107 (9) 4004-4009; (2010)

[Jik01] Jikwang Kim, Jongsung Kim, Younghwa Shin, Youngsoo Yoon. *A study on the fabrication of an RTD (resistance temperature detector) by using Pt thin film.* Korean Journal of Chemical Engineering volume 18, pages61–66 (2001)

[Jin11] Jing Wu, Min Gu, *Microfluidic sensing: state of the art fabrication and detection techniques.* J. Biomed. Opt. 16(8) 080901 (2011)

[Jor08] Jordan M. Berg, Tim Dallas. *Peristaltic Pumps.* Springer Verlag, https://link.springer.com/referenceworkentry/10.1007%2F978-0-387-48998-8_1198 (2008)

[Lip93] Liptak Bela G. *Flow measurement.* Chilton Book Company (1993)

[Mar00] Marc A. Unger, Hou-Pu Chou, Todd Thorsen, Axel Scherer, Stephen R. Quake. Monolithic Microfabricated Valves and Pumps by Multilayer Soft Lithography *Science* Vol. 288, Issue 5463, pp. 113-116. (2000)

[Max20] Maxim Integrated *MAX31865 RTD-to-Digital Converter.* Datasheet https://datasheets.maximintegrated.com/en/ds/MAX31865.pdf (25.11.2020)

[McD99] J. Cooper McDonald, David C. Duffy, Janelle R. Anderson, Daniel T. Chiu, Hongkai Wu, Olivier J. A. Schueller, George M. Whitesides. *Fabrication of microfluidic systems in poly(dimethylsiloxane).* Electrophoresis, Pages 27-40. (1999).

[Mer20] Merck. *Rhodamin B Datasheet.* https://www.sigmaaldrich.com/catalog/product/sigma/83689?lang=de&region=DE (29.11.2020)

[Mes06] Meschede D. *Gerthsen Physik.* Springer Spektrum ed. 23 (2006)

[Min09] Minsoung Rhee, Mark A. Burns. *Microfluidic pneumatic logic circuits and digital pneumatic microprocessors for integrated microfluidic systems.* Lab on a Chip, Issue21, (2009)

[Mir13] Miralles, V.; Huerre, A.; Malloggi, F.; Jullien, M.-C. *A Review of Heating and Temperature Control in Microfluidic Systems: Techniques and Applications.* Diagnostics 3, 33-67. (2013)

[Moo65] G. E. Moore, *Cramming more components onto integrated circuits*, Electronics, volume 38, number 8, April 19, (1965).

[Nei19] Neil Convery, Nikolaj Gadegaard *30 years of microfluidics*, Micro and Nano Engineering, Volume 2, Pages 76-91, ISSN 2590-0072 (2019).

[Ome20] Omega. *Temperatursonden.* https://www.omega.de/prodinfo/Temperatursonden.html (25.11.2020)

[Pam14] Pamela N. Nge, Chad I. Rogers, Adam T. Woolley *Advances in Microfluidic Materials, Functions, Integration and Applications.* Chem Rev. Author manuscript; available in PMC Apr 10. (2014)

[Pcm20] PCmag. *Land Grid Array. https://www.pcmag.com/encyclopedia/term/lga* (29.11.2020)

[Pop19] Jürgen Popp, Sonja Höfer, Thomas G. Mayerhöfer, "Deviations from Beer's law on the microscale – nonadditivity of absorption cross sections", Physical Chemistry Chemical Physics , 21 (19), pp. 9793–9801, (2019)

[Rak20] Rakesh P. Borase, D. K. Maghade, S. Y. Sondkar, S. N. Pawar. *A review of PID control, tuning methods and applications.* International Journal of Dynamics and Control (2020)

[Res20] Resitancewire Hyndman Industrial Products Inc. *Resistance Heating Wire Nickel-Chromium Alloy 80% Nickel /20% Chromium - N8* https://resistancewire.com/uploads/page/ADT2001_12_17_N8_ENG.pdf (28.11.2020)

[RKI20] © Robert Koch-Institut *COVID-19 (Coronavirus SARS-CoV-2)*

https://www.rki.de/DE/Content/InfAZ/N/Neuartiges_Coronavirus/nCoV.html (20.11.2020)

[Rod16] Isaac Rodríguez-Ruiz, Tobias N. Ackermann, Xavier Muñoz-Berbel, Andreu Llobera *Photonic Lab-on-a-Chip: Integration of Optical Spectroscopy in Microfluidic Systems. Anal. Chem. 2016, 88, 13, 6630–6637* (2016)

[Sim20] Simplify3D https://www.simplify3d.com/support/print-quality-troubleshooting/ (27.11.2020)

[Spa20] SparkFun Electronics. *Spectral Triad (AS7265x) Hookup Guide* https://learn.sparkfun.com/tutorials/spectral-triad-as7265x-hookup-guide (25.11.2020)

[SV15] Saggiomo, V. Velders, A. H. *Simple 3D Printed Scaffold-Removal Method for the Fabrication of Intricate Microfluidic Devices. Adv. Sci.*, 2: 1500125. (2015).

[Tec20] TEconnectivity Sensor Soulution. *PT TEMPERATURE SENSOR –PTF FAMILY.* Datasheet (25.11.2020)

[Tej19] Tejvan Pettinger. Reasons for falling price of electronic goods.https://www.economicshelp.org/blog/147811 (2019)

[The11] Svirchuk, Ye.S. ELECTRIC (JOULE) HEATERS. http://www.thermopedia.com/content/719/ Article last modified: 10 February (2011)

[Tip15] Paul A. Tipler; Gene Mosca. *Physik Tipler* ed.7 Springer-Verlag Berlin Heidelberg 1994, 2004, 2009, 2015

[Ven14] Ventola, C Lee. *Mobile devices and apps for health care professionals: uses and benefits.* P & T : a peer-reviewed journal for formulary management vol. 39,5; 356-64. (2014).

[Ver20] Veryst. *Delamination in Microfluidic Valves.* https://www.veryst.com/case-studies/delamination-microfluidic-valves (25.11.2020)

[Vin04] Vincent Studer, Giao Hang. *Scaling properties of a low-actuation pressure microfluidic valve.* AIP Journal of Applied Physics 95, 393 (2004)

[Vil20] Ville Jokinen. "*Capillary action- how contact angle and surface tension are related?*" Biolinscientific, www.biolinscientific.com/blog/capillary-action-how-contact-angle-and-surface-tension-are-related. (23 April 2020)

[Wat96] Watson J.M., Baron M.G. *The behaviour of water in poly(dimethylsiloxane).* Journal of Membrane Science, Volume 110, Issue 1, Pages 47-57 (1996)

[Weh16] Wehner, M., Truby, R., Fitzgerald, D. *et al. An integrated design and fabrication strategy for entirely soft, autonomous robots.* Nature 536, 451–455 (2016).

[Wen20] Wenbin Cao. *The Development and Application of Microwave Heating* https://www.intechopen.com/books/the-development-and-application-of-microwave-heating/microwave-dielectric-heating-of-fluids-in-microfluidic-devices (24.11.2020)

[Whi06] Whitesides, G. *The origins and the future of microfluidics.* Nature 442, 368–373 (2006).

[Xia98] Xia, Younan. Whitesides, George M. *Soft lithography.* WILEY-VCH Verlag GmbH, Weinheim, Fed. Rep. of Germany (1998)

[Yan14] Hui Yan, Hongkai Wu. *Joule Heating and Chip Materials.* Springer, Boston, MA; First Online: 04 May (2014)

[Yua18] Yuan-Sheng Lee, Nirveek Bhattacharjee, Albert Folch. *3D-prined Quake-style microvalves and micropumps.* Lab on a Chip, Issue 8 (2018).

[Zha07] Chunsun Zhang, Da Xing. *Miniaturized PCR chips for nucleic acid amplification and analysis: latest advances and future trends.* Nucleic Acids Res; 35(13): 4223–4237 (2007)

9 List of figures

10 List of abbreviations

Abbreviation	Explanation
3D	Three-dimensional
ABS	Acrylonitrile butadiene styrene
ADC	Analog-to-digital converter
atm	atmospheric pressure
CAD	Computer-aided design
CCD	Charge couple device
CMOS	Complementary metal–oxide–semiconductor
DIN EN	Deutsches Institut für Normung; Europäische Norm
DNA	Deoxyribonucleic acid
EMB3D	Embedded 3D
ESCARGOT	Embedded SCAffold Removal Open Technology
FDM	Fused deposition modeling
GFX	Graphics
IC	Integrated Circuit
IR	Infrared
ISO	International Organization for Standardization
LED	Light-emitting diode
LOC	Lab on a Chip
LGA	Land grid arrays
MEMS	Microelectromechanical systems
NCV	Normally closed valve

NOV	Normally open valve
PCB	Printed circuit board
PCR	Polymerase chain reaction
PDMS	Polydimethylsiloxane
PET	Polyethylene terephthalate
PETG	Polyethylene Terephthalate Glycol
PID	proportional–integral–derivative (for controllers)
PLA	polylactic acid
PMMA	Poly(methyl methacrylate)
PMT	photo multiplier tubes
PT1000	Platinum resistance 1000 Ω at 0 °C
PVA	Polyvinyl Alcohol
PWM	Pulse width modulation
RTD	resistance temperature detectors
SPI	Serial Peripheral Interface
TFT	Thin-film transistor
TLC	Thermochromic liquid crystal
USB	Universal Serial Bus
UV	Ultraviolet

11 Attatchments

Additional information about PDMS:

Note that the surface of PDMS devices or cured PDMS in general is very susceptible to dirt and particles. To clean the component from the outside, it is advisable to use high-quality precision cloths and to dry it with compressed air.

There are a few drawbacks when using PDMS in a combination with certain plastics or rubbers. PDMS does not achieve the optimum properties when it is cross-linked next to these materials. Crosslinking-inhibiting materials are organotin compounds, silicone rubber with organotin catalysts, sulfur, polysulfides, polysulfones, and other sulfur-containing materials, amines, urethanes, amides and azides. When the curing process of PDMS is applied, the crosslink-inhibited areas are still dominated by a state of viscos fluidic PDMS. This behavior can only be compensated if these materials are left out completely.

PDMS Properties:

Density	965 kg/m^3
Boiling point	200 °C
Glass transition	-120 °C
Dielectric strength	19-22 kV/mm
Permittivity ε_r	3,1
Tensile strength	63 Kg/cm^2, 6,2 MPa
Refractive index	1,4225 at 589 nm
Refractive index	1,4118 at 632,8 nm
Refractive index	1,4028 at 1321 nm
Refractive index	1,3997 at 1554 nm
Surface energy	19,9 mJ/m^2

Curing can take place at room temperature or can be accelerated by using higher temperatures:

- Curing time at 25 °C: 48 h.
- Curing time at 100 °C: 35 min
- Curing time at 125 °C: 20 min
- Curing time at 150 °C: 10 min

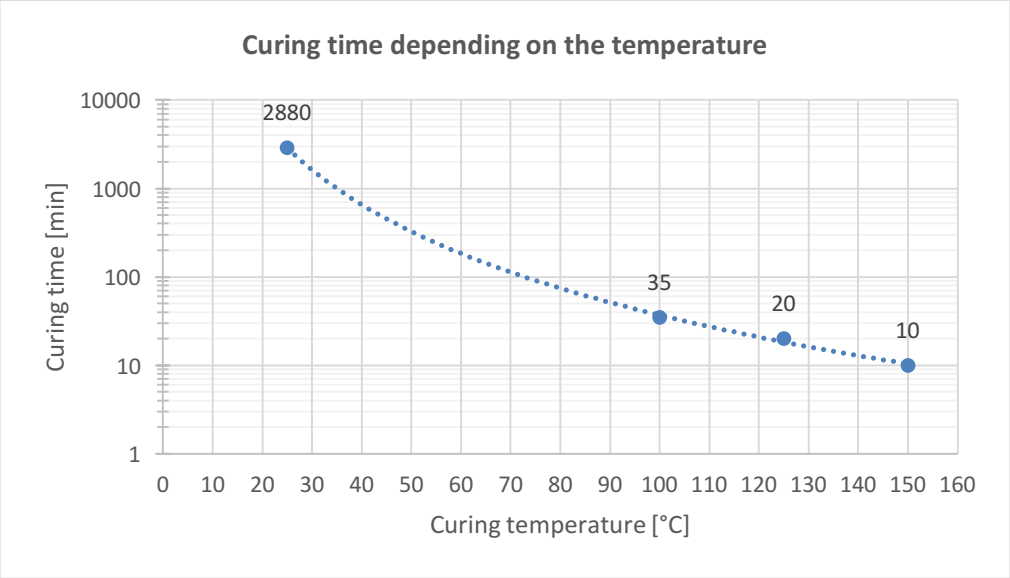

Attachment Figure 1: Curing time dependence on the curing temperature.

Influence of the curing temperature on the mechanical properties

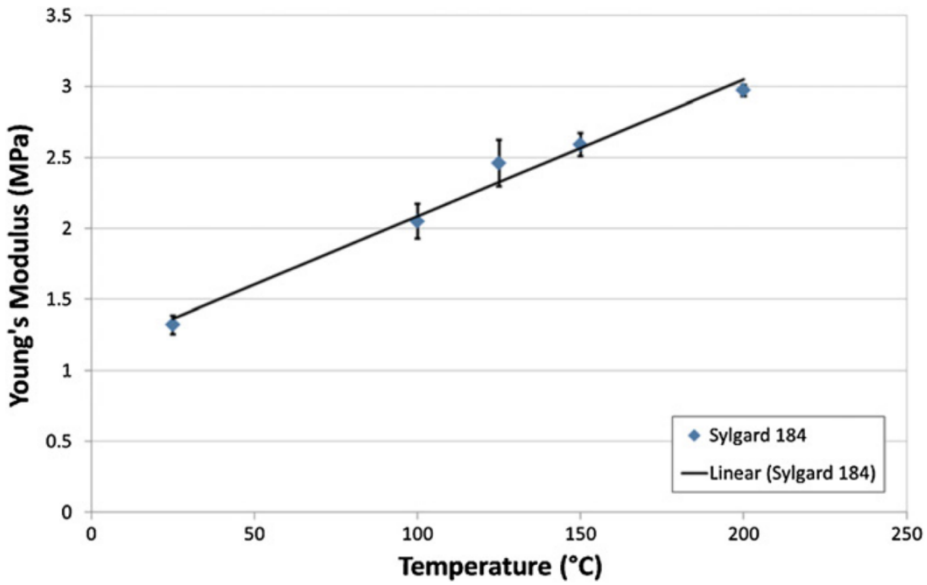

Attachment Figure 2: Youngs modulus dependence on the temperature.

The curing method (whether at room temperature or in the oven) influences the mechanical properties of the PDMS structure.

The higher the curing temperature, the greater the modulus of elasticity (Young's modulus). This means that the resistance that the material offers against elastic deformation increases and the material is therefore more rigid.

Influence of the mixing ratio on the mechanical properties

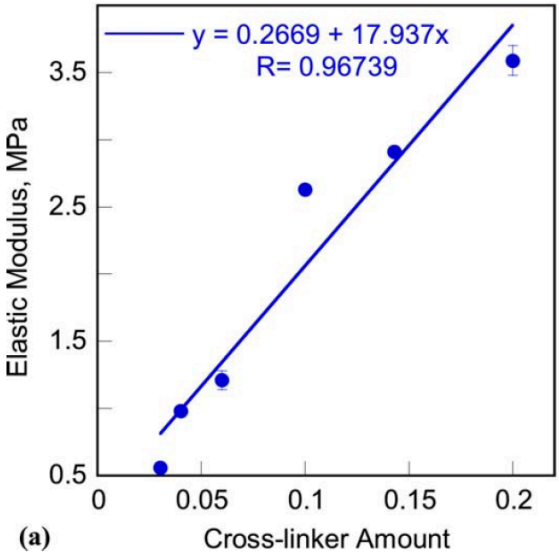

Attachment Figure 3: The modulus of elasticity of PDMS increases with a higher proportion of cross linker and is 3.6 MPa at a ratio of 5: 1. It is reduced to 0.5 MPa at a ratio of 33: 1. The relationship between the ratio of base and hardener to the

If various filler materials, such as highly disperse silicon dioxide, carbon black or metal oxides, are added before vulcanization, the mechanical properties of the polydimethylsiloxane networks can be improved.

Source: https://opus.bibliothek.uni-wuerzburg.de/opus4-wuerzburg/frontdoor/deliver/index/docId/244/file/weh.pdf

.

6-channel spectral sensing prototype

Developed semi-portable prototype, which was fabricated before the 18-channel prototype. This includes a two-way cross-section with incorporated quake valves. One of the valves is still filled with the ABS-scaffold for demonstration purposes.

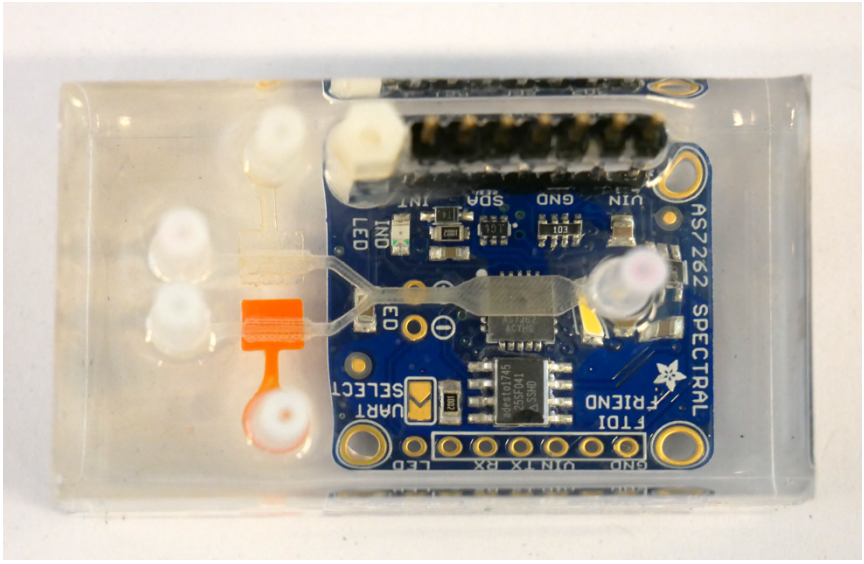

Attachment Figure 4: 6-channel spectral sensing prototype

Peristaltic Pump measurements

Table 1: Conducted pumping rates of the developed peristaltic pump

Frequency	2 bar	2.5bar
5	0,39	0,56
10	0,52	1,04
20	0,91	2,19
30	1,26	2,64
40	1,51	3,45
44	1,27	3,47
48	1,11	3,60
52	1,01	3,35
56	1,09	3,56
60	0,98	2,95
64	1,33	3,98
68	1,44	4,58
72	1,87	4,79
76	1,91	4,19
80	1,63	3,87
100	0,65	3,56
150		2,70
200		0,22

The measurements shown above are calculated through the time it took to fill the measurement body. Each pumping rate reflects the average value of 22 measurements for each frequency. Each single measurement is shown on the next page in a unified graph for each pressure.

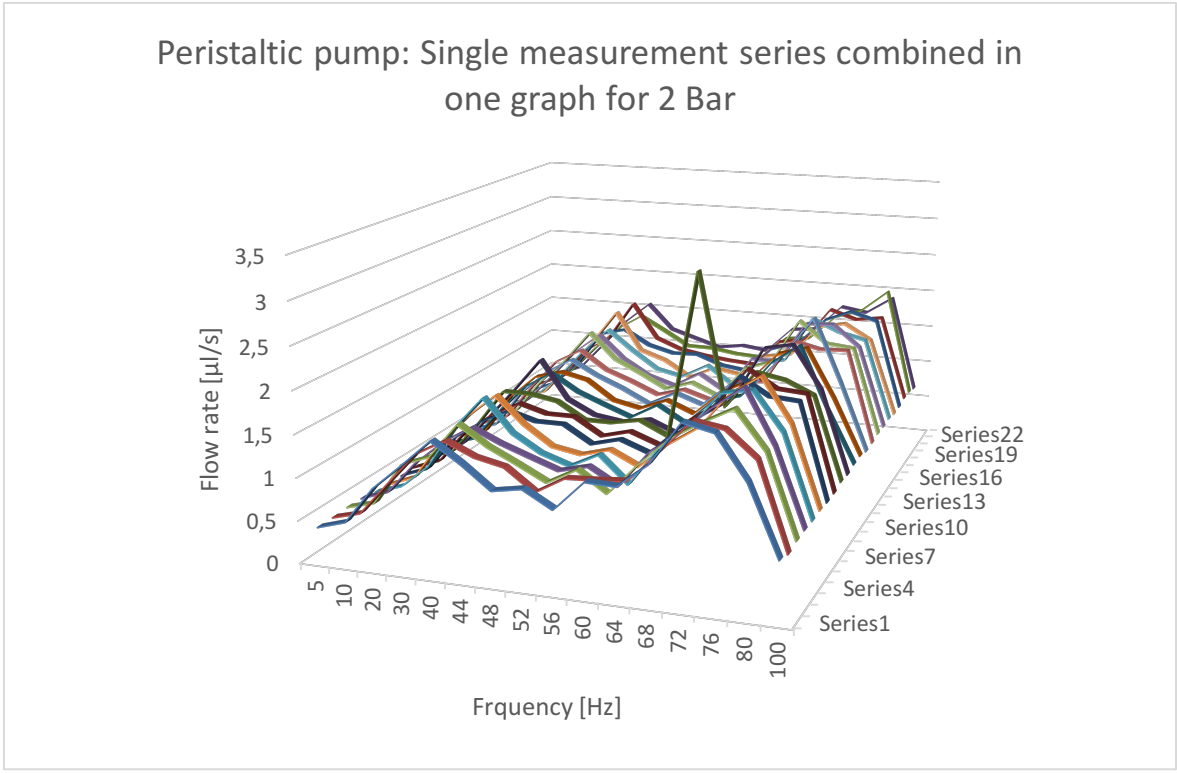
Peristaltic pump: Single measurement series combined in one graph for 2 Bar
Flow rate [µl/s]
3,5
3
2,5
2
1,5
1
0,5
0
5
10
20
30
40
44
48
52
56
60
64
68
72
76
80
100
Frquency [Hz]
Series22
Series19
Series16
Series13
Series10
Series7
Series4
Series1

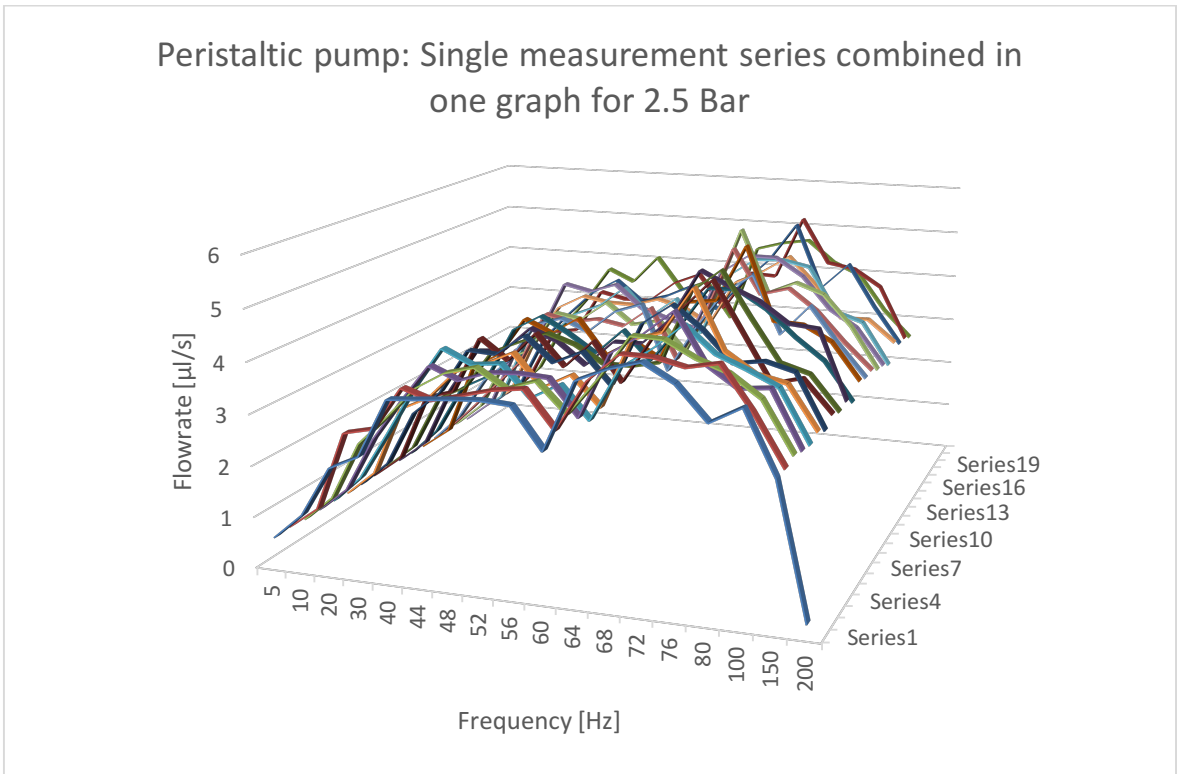
Peristaltic pump: Single measurement series combined in one graph for 2.5 Bar
Flowrate [µl/s]
6
5
4
3
2
1
0
5
10
20
30
40
44
48
52
56
60
64
68
72
76
80
100
150
200
Frequency [Hz]
Series19
Series16
Series13
Series10
Series7
Series4
Series1

Additional information

All additional changes in Arduino code and design files from Autodesk Fusion 360 will be uploaded on the WHS Server. Questions can be directed to the department of microsystem technology.